Investigation of Basin Characteristics: Implications for Sub-basins Level Flood Peak and Vulnerability Assessment

Rajeev Ranjan (engrajeevcivil12@gmail.com)
Indian Institute of Remote Sensing Dehradun Uattarkhand IN https://orcid.org/0000-0003-4939-1340
Pankaj R. Dhote
Indian Institute of Remote Sensing
Praveen K. Thakur
Indian Institute of Remote Sensing
Shiv P. Aggarwal
Indian Institute of Remote Sensing

Research Article

Keywords: Flood vulnerability, Hydrological modelling, Indicator-based method, GIS, Flood peak

Posted Date: June 24th, 2021

DOI: https://doi.org/10.21203/rs.3.rs-588510/v1

Investigation of Basin Characteristics: Implications for Sub-basins Level Flood Peak and Vulnerability Assessment

Rajeev Ranjan[1], Pankaj R. Dhote[1], Praveen K. Thakur[1], Shiv P. Aggarwal[1]

[1]Indian Institute of Remote Sensing, ISRO, Dehradun, Uttarakhand, India, 248001

Corresponding author: Pankaj R. Dhote (pdh@iirs.gov.in)

Abstract

Flood vulnerability is a significant component in assessing the probable degree of damage to various exposures in hazard conditions. In this study, a semi-distributed event-based hydrological model and indicator-based method were applied to evaluate the sub-basin level flood vulnerability using the Geographical Information System (GIS). The flood peak discharge of each sub-basin corresponding to the 2014 extreme flood of the Jhelum river was related with different sub-basins characteristics (terrain, hydrological, land use and soil) using a theoretical framework under an indicator-based method. The calibrated (2014) and validated (1992, 1997) hydrological model showed Nash-Sutcliffe Efficiency (NSE) of 0.98 and (0.99, 0.99) at relatively upstream gauging station Sangam against optimized Curve Number (CN) scaling factor of 0.98. The Anantnag and Kulgam districts, exhibiting multiple sub-basins contributing to the Sangam gauging station, are falling into a highly vulnerable category located in the Jhelum basin's southern part, Greater Himalayan Range. It was also revealed that sub-basins at the upstream of the Jhelum basin are more

vulnerable compared to downstream area, where sub-basin W810 (Greater Himalayan), Anantnag district draining at Sangam gauging site is found as most vulnerable among the all other sub-basins. However, hydrological characteristics control the most vulnerable sub-basin peak discharge rather than other characteristics such as terrain, soil, or Land Use. Outcomes of the study will be helpful in prioritizing the flood mitigation planning not only with respect to the hydrological boundary (sub-basin level) but also with administrative district boundaries. The proposed method is generic and can be applied to any flood-prone river basin.

Keywords: Flood vulnerability, Hydrological modelling, Indicator-based method, GIS, Flood peak

1. Introduction

Flooding is recurrent phenomena amongst all-natural catastrophe (earthquake, landslides, forest fires etc.) (Dhar and Nandargi 2003; Jonkman 2005; Aggarwal et al. 2009; Ahmad et al. 2018) that solemnly affects society leading to loss of lives and properties. Natural catastrophes like debris flows and floods are the serious threat for the livelihood of the hilly and mountainous region (Watson and Haeberli 2004; Meraj et al. 2015). In the recent past years, Himalayan regions have encountered major appalling calamitous floods such as floods in Tirthan River, Himachal Pradesh flood (2005); Kosi River, Bihar flood (2008); a flash flood in Leh (2010); floods in Ganga River (2010); Brahmaputra River, Assam flood (2012; a flash flood in Kedarnath, Uttarakhand (2013); and flood in Jhelum River, Jammu and Kashmir (2014) (Bhatt et al. 2017; Dhote et al. 2019; Thakur et al. 2019). Flood is a menace to sustainable development in the Himalayan regions (Ives 2004; Bhatt et al. 2017). There is a need for sub-basin level flood peak characterization using hydrological and geospatial model inputs to facilitate prompt environmental planning in flood-prone areas. This

will establish the direct link between physical phenomenon (flood) and the land attributes (Halwatura and Najim 2013) and atmospheric parameters to minimize the flood damage.

The unavailability or limited availability of observational data are the big hindrance in the path of solving real world physical problems using model-based approach (Chaponnière et al. 2008; Keshari et al. 2010; Romshoo et al. 2012; Meraj et al. 2015). The empirical methods, unit hydrograph, rational formulas, watershed models and flood frequency technique are the conventional techniques to estimate the peak design floods (Halwatura and Najim 2013; Aggarwal et al. 2019). The basin characteristics and the required hydrological responses in the basin are the measures for model selection (Hunukumbura et al. 2008; Chouksey et al. 2017). The commonly used Hydrological models for the estimation of precipitation based hydrological responses are, Hydrologic Engineering Centre – Hydrological Modelling System (HEC-HMS), SWAT (Soil Water and Assessment Tool), VIC (Variable Infiltration Capacity), Geomorphological Instantaneous Unit Hydrograph (GIUH), University of British Colombia Watershed Model (UBCWM) etc. (Morid et al. 2002; Milewski et al. 2009; Beyene et al. 2010; Loukas and Vasiliades 2014; Nikam et al. 2018; Thakur et al. 2020). U.S. army corps has developed the physical hydrological model i.e. HEC-HMS (Engineers 2008; Feldman 2000; Scharffenberg & Fleming 2006). It is commonly used to simulate or analyze the event-based hydrological responses such as flood discharge estimation, flood frequency, reservoir spillway capacity, flood forecasting, urban flooding, stream restoration etc. (Feldman 2000; Tang et al. 2018; Chang et al. 2017; Thakur et al. 2020). Huang et al. (2016) has used the event-based hydrological model to identify the dominant hydrological process and suiatble model strategy for the semi-arid catchments. However, fast, accurate and low-cost simulation capability of Artificial Intelligence (AI)-based data-driven models, emerged as an alternative for the conventional method of stream flow simulations (Nourani

et al. 2011; Mehdizadeh et al. 2019). Shamseldin et al. (2007) has attempted to combine the modelled runoff from the different rainfall-runoff models using the comparative study of three other AI-based models such as Artificial Neural Ntework (ANN), Multi-layer Perceptron (MLP), and Radial Basis Functional Neural Network (RBFNN), respectively. Talei and Chua (2012) has studied the influence of lag-time using the event-based rainfall-runoff modelling based on data-driven techniques. He et al. (2014) have simulated the river flow using AI-based hybrid models such as ANN, Adaptive Neuro fuzzy Inference System (ANFIS), and Support Vector Machine (SVM), respectively. Young and Liu (2015) have implemented the hybrid of HEC-HMS (physical-based) and ANN (AI-based) models to develop the rainfall-runoff model to simulate the runoff during Typhoon events.

But, the wide applications of HEC-HMS modelling were also reported in the previous studies (Álvarez et al. 2008; Aggarwal et al. 2019). Halwatura & Najim(2013) focuses on simulation of runoff in a tropical catchment using HEC-HMS model. Abushandi and Merkel(2013) study implemented the HEC-HMS and IHACRES (Identification of unit Hydrographs and Component flows from Rainfall, Evaporation and Stream flow data) modelling to establish the rainfall runoff relations in an arid region of Jordan, estimation of snow-melt using temperature index method in HEC-HMS model (Bobál et al. 2015). Gebre(2015) has simulated the rainfall runoff for upper Blue Nile River basin using HEC-HMS model. Some of the studies where HMS model was applied are; a study by Ibrahim-Bathis and Ahmed (2016) states an integrated application of HEC-HMS model and SCS-CN in ungauged Doddahalla agriculture watershed; rainfall-runoff modelling accounting soil moisture in HEC-HMS model (Razmkhah et al. 2016a), and event based rainfall-runoff modelling (Razmkhah 2016b; Chang et al. 2017). A review on advancements in techniques of flood forecasting is done by the integration of rainfall-runoff modelling and remote sensing based

soil moisture data (Li et al. 2016). Koneti et al. (2018) utilized HEC-HMS model to study the impact of change of Land Use Land and Land Cover change on the dynamics of runoff in Godavari River basin.

Perhaps, the combination of two or more technologies is writing the script of a new era of innovations and advancements in the research areas. Integration of Geographic Information System (GIS) with such types of hydrological models not only enhancing the research outcomes but also shows the advancement of technologies in the field of hydrology. Various studies in the past have revealed the strong and valuable existence of GIS in the domain of disaster risk assessment that includes the hazard, vulnerability or susceptibility and risk assessment of catastrophes like floods and landslides using their indicators termed as "indicator-based approach" (Nasiri et al. 2016; Biswas et al. 2021). Multi criteria-based Decision Making (MCDM) Model such as Analytical Hierarchical Process (AHP) is one of the most famous techniques in the field of hazard assessment and in the identification of susceptible or vulnerable areas with the combination of GIS (Chen et al. 2015). Stefanidis and Stathis (2013) have used the indicator-based approach to assess the flood hazard zones in northern Greece using MCDM based AHP and GIS. . Integrated flood hazard assessment based on spatial ordered weighted averaging method considering spatial heterogeneity of risk preference was completed using the Indicator-based GIS approach by (Xiao et al. 2017). Chen et al.(2015) made indicator-based flood hazard assessment in the Kujukuri Plain of Chiba Prefecture, Japan, based on GIS and multi-criteria decision analysis. Singh et al. (2020) used GIS-based multi-criteria technique to identify the flash-flood prone reaches in Beas river basin. Vignesh et al. (2020) have implemented MCDM based AHP and GIS combined approach for the identification of suspectibile flood zones in the flood-prone regions of Kanyakumari district using the flood indicators (or influencing factors or triggering factors). Various literatures are also

113 available on the application of AI-based models in the field of flood hazard predictions or or
114 susceptibility mapping such as Hong et al. (2018), in their study, used MCDM based Stepwise
115 Assessment Ratio Analysis (SWARA) and a hybrid of ANFIS (AI-based) model with Genetic
116 Algorithm (GA) and Differential Evolution (DE) algorithm for the flood susceptibility mapping of
117 Hengfeng County in Jiangxi Province, China; Falah et al. (2019) used the GIS and combined ANN
118 as an AI-based model for the flood susceptibility mapping in data-scarce urban regions of Emam-
119 Ali town, in Mashhad located in Khorasan Razavi Province, Iran; and Termeh et al. (2018) has done
120 flood susceptibility using the ensemble of AI-based ANFIS and metaheuristic models in the Jahrom
121 Township Fars Province.
122 There are several approaches other than MCDM that have been revealed in the available literatures
123 for establishing the functional relationships among the vulnerability and their elements or indicators
124 as 1. Deductive (z-score transformation, min-max transformation, maximum value or ratio value
125 transformation, etc.) and 2. Inductive approaches (spectral normalization, weight normalization,
126 etc.) to standardize or normalize or rescale them between 0 to 1 (Clark et al. 1998; Wu et al. 2002;
127 Cutter et al. 2003; Yoon 2012; Miyato et al. 2018). However, Kumar et al.(2016); Žurovec et
128 al.(2017) and Choudhary and Badal(2018) have used one of the famous deductive approach
129 developed by Human Development Index (HDI), United Nation Development Program (UNDP's)
130 (Xs et al. 2006) using the functional relationships between the vulnerability and their indicators.
131 Deep learning neural networks have evolved as one of the very effective techniques in this field
132 during the recent years (Huang et al. 2017; Miyato et al. 2018; Sun et al. 2020).
133 Kashmir valley, a part of Himalayan regions is vulnerable to various kinds of natural calamities
134 especially flood due to its mountainous terrain, heavy rainfall including cloud-burst and excessive
135 snow/glacier melting (Bilham et al. 2010; Ebi et al. 2007; Ganju & Dimri 2004; Maqsood et al.

2010; Meraj et al. 2015; Ray et al. 2009; Romshoo et al. 2012). The total geographical area of India prone to the flood is approx. 45.640 million hectares, out of which about 0.514 million hectares area lie in the Jammu and Kashmir i.e. 2.3 % of its total geographical area (Planning Commission 2011). Climate change has increased the frequency of intense rainfall and flood events around the globe including the North-West Himalayas (Mishra & Srinivasan 2013; Murari et al. 2001; IPCC 2007; Dhote et al. 2018; Nikam et al. 2018; Romshoo et al. 2018; Thakur et al. 2019). The history revealed that in the past, Kashmir valley has encountered many causalities that caused loss of livelihood and properties (Singh and Kumar 2013; Meraj et al. 2015) due to the major flood events (as 879 AD, 1841, 1893, 1903, 1929, 1948, 1950, 1957, 1959, 1992, 1996, 2002, 2006, 2010, 2014 etc.,) (Romshoo et al. 2018), landslides, earthquakes and avalanches (Lawrence 1895; Singh and Kumar 2013). The Kashmir 2014 flood (3262.60 cumec) was similar to 1903 and 1959 floods according to the people of Kashmir (Lawrence 1895; Bhatt et al. 2017; Romshoo et al. 2018) . The heavy and intense rainfall from 1st Sep 2014 to 6th September 2014 led to the worst flood in the Kashmir valley (Kumar and Acharya 2016; Romshoo et al. 2018). The current study emphasizes on the combined utilization of hydrological modelling and indicator-based methods to assess the sub-basins level flood vulnerability in the Jhelum River basin.

2. Study area and data

2.1 Description of the study area: Jhelum River basin

Fig. 1 depicts the geographical location of Jhelum river basin (9,472.14 Km^2) with an outlet at the Asham, Bandipora district of Jammu and Kashmir. Jhelum River originates from the spring called 'Chasma Verinag' lies in the Anantnag district. It is commonly known as Hydaspes in Greek, Vitasta in Sanskrit and Vyath in Kashmir. Jhelum River, a major tributary of Indus River acts as a

159 ridge rope for the livelihood of Kashmir valley. The Jhelum River basin system comprises of
160 various tributaries, some of them flow from the Pir Panjal range and join the river on left bank while
161 remaining meet the river on right bank, draining from the Himalayan range. High elevation
162 difference can be observed in the basin varying from 1550 to 5347 m. The bowl shape of Kashmir
163 valley is filled with alluvium having steep slopes that may lead to disastrous flood, post heavy
164 rainfall storm of 1-2 hours (Dhar et al. 1982; Ganjoo 2014; Kumar and Acharya 2016).The
165 reclamation of floodplains and low lying areas for the urbanization and agriculture due to the
166 increased population density have increased the flood risk in the Jhelum basin (Census of India
167 2011; Romshoo et al. 2012). The prominent Land Use and Land covers (LULC) and soil types are
168 the measure of surface flow present in the valley, governing the sub-basins flow in the basin. The
169 region has varied LULC types such as Built-up (BU-2.19%), Crop Land (CL-37.51%), Evergreen
170 Broadleaves Forest (EBF-34.40%), Waterbody (WB-1.94%), Glacier/Snow-Ice (GL/SI-20.62%),
171 and Shrubland/Wasteland (SL/WL-3.34%), see Fig.3 and Fig.4. The percentage of Hydrological
172 Soil Group (HSG) in the study area as A-48.78%, B-25.32%, C-24.42%, and D-1.48%, depict the
173 primarily soil types in the region, see Fig.4.
174 The average annual precipitation in the valley is about 650 mm, as far as the outer hilly region
175 concerned, it receives more than the central valley (Ahmad et al. 2018). The mean temperature in
176 the valley varies from 7.5^{o} Celsius in the winter to 19.8^{o} Celsius in the summer season (Bhat et al.
177 2019). The Kashmir valley receives the heavy snowfall in mountainous regions and rainfall in the
178 adjoining plain areas due to two types of meteorological systems named as the barotropic southwest
179 monsoon and baroclinic extra tropical western disturbances (Sikka 1999; Dhar and Nandargi 2005;
180). These disturbances repeat approximately 4 to 5 times per month during monsoon and nearly 6 to
181 7 times per month in winter (Nandargi and Dhar 2011; Kumar and Acharya, 2016). The more

activeness of western disturbances in the winter and spring seasons as compare to summer results into the most amount of precipitation during winter and spring (Bhutiyani et al. 2010; Dar et al. 2015).

Fig. 1. Jhelum River basin with outlet, drainages, sub-basins & gauging sites

2.2 Data and tools used

The Advanced Land Observing Satellite (ALOS) Phased Array type L-band Synthetic Aperture Radar (PALSAR) Radiometrically Terrain Corrected (RTC) Digital Elevation Model (DEM) acquired from the Alaska Satellite Facility was used in the present study for the DEM hydro-preprocessing. The Indian Space Research Organisation-Geosphere Biosphere Program (ISRO-IGBP) 2005, LULC and the National Bureau of Soil Survey and Land Use Planning (NBSSLUP), soil data were used to prepare the Curve Number (CN) Map. The gridded daily rainfall of Indian Meteorological Department (IMD) of the monsoon seasons (1992, 1997, and 2014) were used as the meteorological input in the hydrological model to simulate the flood hydrographs. Tropical Rainfall Measuring Mission (TRMM) 3-hourly rainfall (Sep 2014) was also used in this study to find the basin lag or lag time (T_{lag}) in the river flow induced after the heavy rainfall event of Sep 2014. The observed discharge of three gauging stations i.e. Sangam, RamMunshi Bagh and Asham was procured from the Irrigation and Flood control Department, Jammu and Kashmir for calibration and validation of the model. The detail overview of database used in the present study is shown in the Table 1. Tools and software used in the study for the processing of input data are as: (1) HEC-Geospatial Hydrologic Modeling System (GeoHMS): an extension of ArcGIS 10.3 used for the DEM hydro processing and the generation of basin characteristics to create the setup files for the

HEC-HMS 4.3, (2) HEC-HMS 4.3: used for the simulation, calibration, sensitivity, and the validation analysis of the model, Arc-GIS 10.3 and Erdas Imagine 2014: used for creating the geospatial environment for the processing the GIS vector and raster image data, respectively.

Table 1: Datasets used in the study

3. Methodology

The methodology adopted to assess sub-basin level flood vulnerability is divided into two primarily sections: (1) setup of hydrological model to extract sub-basin characteristics and flood peak estimation; (2) identification of vulnerable sub-basins by relating flood peak discharge with sub-basin characteristics using indicator-based GIS method. The outline of implemented methodology is shown in Fig.2. The above two sections have been briefly explained in following subsections.

Fig. 2. Methodology flowchart

3.1 Hydrological modeling using HEC-HMS

3.1.1 Basin characteristics estimation using HEC-GeoHMS

The HEC-Geo HMS interface, an extension of ArcGIS 10.1 was used to establish semi-distributed framework (Feldman 2000; ESRI 2011) for the Jhelum River basin. The user-friendly interface allows the easy generation of basin characteristics for the hydrological model using topographic data. The ALOS PALSAR RTC product was pre-processed that includes the processes such as fill sink, flow direction, flow accumulation, stream definition, stream link, catchment grid delineation, catchment polygon processing, drainage line processing and adjoint catchment processing. The

228 eight direction (D8) flow model algorithm was used for the preparation of flow direction (Jenson
229 and Domingue 1988). The threshold value used for defining the streams was 100 km^2, the stream
230 network was able to mimic the actual drainage pattern as seen in the satellite imagery. The gauging
231 station Asham was defined as an outlet to delineate the Jhelum River basin. For each sub-basin
232 different catchment characteristics were estimated such as river slope, river length, basin slope,
233 longest flow path, basin centroid and centroid longest flow path.
234

235 **3.1.2 Hydrological model (HEC-HMS) configuration**

236 The extensively used hydrological model HEC-HMS, developed by the U. S. Army Corps of
237 Engineers Hydrologic Engineering Center was used to simulate flood hydrographs in Jhelum River
238 basin (Engineers 2008). In order to run the simulation, the model is needed to be configured with
239 well-defined processes such as (1) estimation of initial abstraction/loss (loss model), (2)
240 transformation of excess rainfall into Unit Hydrograph (UH) (transform model), (3) conversion of
241 Direct Runoff Hydrograph (DRH) into flood hydrograph (base flow model), and (4) generation of
242 flood hydrographs at various river sections (routing model); the execution of these processes depend
243 on the algorithms given in the model (Feldman 2000; Scharffenberg and Fleming 2006;).
244 The Soil Conservation Service (SCS)-Curve Number (CN) method was opted for the loss model to
245 estimate the accumulated rainfall excess (Mishra et al. 2004; Soulis and Valiantzas 2012; Prakash
246 and Abhisek 2016; Koneti et al. 2018). The SCS-CN method for the computation of accumulated
247 precipitation excess in the form of stream flow volume depends (Ibrahim-Bathis and Ahmed 2016)
248 on the soil cover i.e. HSG, cumulative rainfall, antecedent moisture and land use. SCS has
249 developed the empirical relationship between initial abstraction (I_a) and potential maximum
250 retention (S) (equation 1) (NRCS 1986).

$$\mathbf{P_e} = \frac{(\mathbf{P}-\mathbf{I_a})^2}{(\mathbf{P}-\mathbf{I_a})+\mathbf{S}} \quad (1)$$

where:

P_e = accumulated precipitation excess at time t

P = accumulated rainfall depth at time t

I_a = the initial abstraction (initial loss)

S = potential maximum retention

$$\mathbf{I_a} = \mathbf{0.2\,S} \quad (2)$$

$$\mathbf{P_e} = \frac{(\mathbf{P}-\mathbf{0.2S})^2}{(\mathbf{P}-\mathbf{0.8S})+\mathbf{S}} \quad (3)$$

where,

$$\mathbf{P \geq 0.2S}$$

$$\mathbf{S} = \frac{\mathbf{25400}}{\mathbf{CN}} - \mathbf{254} \quad (4)$$

The depression storage, interception and the infiltration during early stage of storm constitute the initial abstraction (I_a) (Ponce 1994). The imperviousness of the region controls the amount of initial abstraction. More is the built-up percent, more is the imperviousness and less will be the amount of initial abstraction and the impervious percent of each sub-basin was calculated by the percent of LULC present (NRCS 1986; Garg et al. 2017). The sub-basin wise LULC percent statistics, depict the high built percent in sub-basin W910 that clearly signifies its high impervious percent and hence, less initial abstraction in this sub-basin (Fig.3.). The potential maximum retention is a potential measure of basin for the extraction and retention of the storm precipitation depends on the CN. The mean CN value for each sub-basin was extracted from the CN raster grid as shown in the Fig. 4. The CN raster was generated by the integration of soil (HSG), LULC and slope in the HEC-

GeoHMS interface of Arc-GIS. The CN values of different LULC classes in HSG were taken from the standard table called CN look up table as given in the Table 2 (NRCS 1986; Schwab et al. 2005). HSG characterizes the soil types into four classes i.e., A, B, C, and D based on their hydrological properties (runoff, infiltration, etc.), where D represents the soil having maximum surface runoff and minimum infiltration capacity, A is the soil with minimum surface runoff and maximum infiltration capacity, but C, and D, soil types lie in between A and D, respectively (NRCS 1986; Subramanya 2008).

Fig. 3. LULC percent of each sub-basin

Table 2: CN values for different HSG group according to United States Department of Agriculture (USDA) TR 55

The rainfall excess obtained from the loss model was transform into the surface runoff using the SCS UH technique in the transform model (Feldman 2000; Reshma et al. 2010; Hari et al. 2011). The mathematical formulation of SCS UH states that the peak of UH is a function of watershed area and time of peak (T_p). The time of peak depends on the excess precipitation and T_{lag}, whereas the lag time is a function of time of concentration or travel time (T_c) (NRCS 1986; Feldman 2000). The TR-55 working sheet obtained during the configuration of model involves the calculation of T_c. The T_c of each sub-basin is the sum of travel time obtained during the sheet flow, shallow concentrated flow and channel flow that depends on the basin physical characteristics. The details of the watersheds characteristics involved in the TR-55 working sheet such as sheet flow characteristics, shallow concentrated flow characteristics and channel flow characteristics are

295 discussed in the USDA and National Resource Conservation Soil (NRCS) TR-55 technical release
296 (NRCS 1986). The DRH peak derived from the transform model was converted into the peak of
297 flood hydrograph using the base flow model. The base flow is the delayed sub-surface flow occurs
298 above the Ground Water Table (GWT) was estimated by Straight Line method (Subramanya 2008).
299 Muskingum Cunge and lag method were opted in routing model to derive the flood hydrograph at
300 the various sections of the reach (Feldman 2000; Subramanya 2008; Hari et al. 2011;). Muskingum
301 Cunge method is a hydraulic method of routing which involves the continuity and the momentum
302 equation along with the equation of motion of unsteady flow i.e. St. Venant equation, whereas lag
303 method routes the flow with the T_{lag} provided in the specific reaches before the stations (Feldman
304 2000; Subramanya 2008; Reshma et al. 2010). T_{lag} is the time difference in the peak of rainfall and
305 peak of discharge of the event (or delay in the event peak flow) (Subramanya 2008).
306
307 **Fig. 4.** LULC, Soil, HSG and CN Map of Jhelum basin
308
309 **3.1.4 Construction of meteorological forcings and the simulation run**
310 The meteorological forcing is one of the most important controlling indicators that governs the
311 hydrological model. The rainfall was acquired from IMD for the monsoon seasons (June-
312 September) of the year 1992, 1997, and 2014. The configured hydrological model was simulated
313 using constructed meteorological forcing for the calibration and validation. The current research
314 carried out simulations for the monsoon periods of the years 1992, 2014, and 1997 where, the model
315 calibration was done for the year 2014 and validation for the years 1992 and 1997, respectively.
316 The flood peaks discharges were estimated for each sub-basin using 2014 extreme rainfall as input
317 forcing.

318

319 **3.2 Identification of vulnerable sub-basins using indicator-based GIS method**

320 This section includes the framework for spotting the vulnerable sub-basins. In order to locate such
321 sub-basins, the current framework is divided into two segments: 1) vulnerability approach, and
322 2) threshold selection criteria to classify the sub-basins into low and highly vulnerable.

323

324 **3.2.1 Vulnerability approach**

325 It is the two-steps approach: 1) the estimation of normalized scores (0-1) of vulnerability
326 indicators and sub-indicators using the functional relationship (positive and negative) between
327 the vulnerability and their indicators, and 2) the computation of sub-basin wise vulnerability.
328 Normalization is the process of making quantities comparable to each other by making them
329 unitless and rescaling to the same range (in this case, 0-1), since initially all the indicators have
330 different units and scale (Yoon 2012; Žurovec et al. 2017).
331 The present work had used an internationally recognized Human Development Index (HDI),
332 United Nation Development Program (UNDP's), 2006 (Birkmann 2006; Xs et al. 2006) min-max
333 linear transformation, a deductive approach for the computation of normalized scores of
334 vulnerability indicators and sub-indicators (Wu et.al. 2002; Yoon 2012; Cutter et.al. 2003).
335 Previous studies have also revealed the existence of this adopted methodology framework for the
336 assessment of vulnerable areas in the different scientific fields (Yoon 2012; Behanzin et al. 2016;
337 Kumar et al. 2016; Žurovec et al. 2017; Choudhary and Badal 2018). In this approach, the
338 functional relationship is based on the theoretical understandings only, where the positive and
339 negative relation signifies the direct and inverse relation (Wu et al. 2002; Cutter et al. 2003; Yoon
340 2012). In this case, sub-basins characteristics (terrain, hydrological, land use and soil) that have

341 direct or inverse relation with the sub-basins flood peaks were treated as vulnerability indicators
342 to establish the functional relationship with the vulnerability. Since, more is the food peak, more
343 will be the sub-basins vulnerability. Further, these characteristics were classified into the sub-
344 characteristics that help in demonstrating a strong theoretical functional relationship
345 understanding with vulnerability than the previous one. Slope and elevation are terrain
346 characteristics have positive (or direct) relation with the flood peaks (Cunge 1969; NRCS 1986;
347 Subramanya 2008; Yalcin 2020). CN, Long Period Average (LPA) rainfall (1970-2015), peak
348 discharge (flood peaks at Sangam, RamMunshi Bagh and Asham are 10, 100 and 200 years return
349 period, respectively during Jhelum 2014 flood events) (Bhat et al. 2019) per unit area, and CN
350 belong to the hydrological characteristics have positive relation with flood peaks except T_c that
351 has negative (or inverse) relation (NRCS 1986; Bosznay 1989; Ponce 1994; Stewart et al. 2012;).
352 Land Use characteristics such as BU, WB and GL/SI have positive relation with flood peaks
353 where EBF, CL, and WL/SL have negative relation that depends on the imperviousness of the
354 LULC (Subramanya 2008; Brody et al. 2014; Sanyal et al. 2014; Garg et al. 2017; Mousavi and
355 Rostamzadeh 2019). For soil characteristics HSG A, B, C, and D were considered where A and
356 B have negative relation, but C and D have positive relation with the flood peaks (NRCS 1986;;
357 Kim and Lee 2008; Stewart et al. 2012; Costache et al. 2020). Characteristics and sub-
358 characteristics of sub-basins and their relationships with the flood peaks are shown in Table 3.
359 Selection criteria for these characteristics were based on the data availability and the scientific
360 literature reviews (Subramanya 2008; D'Asaro and Grillone 2012; Sanyal et al. 2014; Yan et al.
361 2015; Abdulkareem et al. 2018; Jaafar et al. 2019; Mousavi and Rostamzadeh 2019; Sadek et al.
362 2020; Costache et al. 2020).
363

364 **Table 3**: Basin characteristics and their relationship with peak runoff

365

366 HDI, UNDP's, 2006, mix-man linear normalization method for the positive and negative function
367 relationships of vulnerability indicators with vulnerability (Birkmann 2006; Xs et al. 2006; Yoon
368 2012) are discussed in the equations 5 and 6, respectively.

369 $$\mathbf{V_{ij}} = \frac{\mathbf{X_{ij} - Min\ X_i}}{\mathbf{Max\ X_i - Min\ X_i}} \quad (5)$$

370 $$\mathbf{V_{ij}} = \frac{\mathbf{Max\ X_i - X_{ij}}}{\mathbf{Max\ X_i - Min\ X_i}} \quad (6)$$

371 where,

372 $\mathbf{V_{ij}}$ stands for the normalized vulnerability score regarding sub-indicators (i) for the sub-basins
373 (j);

374 $\mathbf{X_{ij}}$ stands for the observed value of the same component for the same sub-basins;

375 $\mathbf{Max\ X_i}$ and $\mathbf{Min\ X_i}$ stand for the maximum and minimum value of the observed range of values
376 of the same component for all the sub-basins.

377 The obtained normalized values of the sub-characteristics were averaged for each sub-basin to
378 obtain normalized score of the sub-basins characteristics as:

379 $$\mathbf{AI} = \frac{\sum_i^n \mathbf{x_{ij}}}{\mathbf{N}} \quad (7)$$

380 where,

381 **AI** being the average index of each sub-basin's vulnerability elements, **N** = the sum of the index
382 and $\mathbf{X_{ij}}$ = the value of the index.

383 The overall Vulnerability Index (VI) scores (Fig.10) for each sub-basin was calculated by
384 weightage linear sum of sub-basins indicators:

385 $$\mathbf{VI} = \sum_i^n \mathbf{V_i W_i} \quad (8)$$

where,

$\mathbf{V_i}$ is the averaged normalized score of each basin's characteristics and $\mathbf{W_i}$ is their weights used in this research.

In this case, equal weightage (W_i = 0.25) were given to the basins characteristics to identify the dominant basins characteristics also without any unfairness. Hence, the high averaged normalized score values of the basin characteristics will represent their most dominant parameters influencing their respective flood peaks. Higher the VI scores of sub-basins, the chance of their vulnerability will be more (Birkmann 2006; Behanzin et al. 2016). The final obtained VI scores of the sub-basins were used to produce the vulnerable sub-basin map (Fig.12a) using the Arc-GIS software by converting the vector into polygon.

Identification of vulnerable districts (Fig.12b) were also done using the area percent contribution of vulnerable sub-basins to each district and the calculated VI scores of respected districts shown in the Table 7 and Fig. 13, respectively. The VI scores for each district ($\mathbf{VI_d}$) was calculated using the area weightage method.

$$\mathbf{VI_d} = \sum_{i}^{n} \mathbf{A_i}\,\mathbf{VI_i} \quad (9)$$

where,

$\mathbf{A_i}$ = area percent of low or highly vulnerable sub-basins of the respective district

$\mathbf{VI_i}$ = VI scores of low or highly vulnerable sub-basins of the respective district

3.2.2 Threshold criteria

The current section emphasized the methods adopted for deciding the threshold VI score to classify the sub-basins between low and highly vulnerable. Present research has used three different scientific techniques for this purpose such as: 1) Mean method, 2) Natural breaks (Jenks) method,

409 and 3) Standard deviation method, respectively to find the Optimal Threshold Value (OTV) (Chung
410 and Lee 2009; Bhattacharya et al. 2020; Singh et al. 2020), a minimum value above which the
411 maximum of given regions become vulnerable. In this case, VI score (0.457) is considered as OTV
412 (derived from the standard deviation method), see Fig.11 for the classification of sub-basins into
413 low and highly vulnerable (Fig.12).
414 Mean method of finding OTV is the average of the all the obtained data values. But Jenks (1967)
415 natural breaks classification is the method for best arrangement of values into different classes
416 identifies the breakpoints by looking for groups and patterns inherent in the data(Ayalew 2004;
417 Stefanidis and Stathis 2013; Balasubramanian et al. 2017). It minimizes and maximizes the average
418 deviation of each class from the class mean and from the other groups means, respectively i.e.
419 minimize the variance within the class but maximize the variance between classes (Jenks, 1967).
420 Standard deviation method is based on the normal distribution signifies the extent of diversion of
421 attribute's values from mean of all the values that creates the class breaks with an equal proportion
422 of standard deviation generally one, one-half, one-third, and the one-fourth using the mean and
423 standard deviation from the mean (Stefanidis and Stathis 2013; Rahadianto et al. 2015).
424

425 **4. Results and discussion**

426 This section discusses the calibration and sensitivity of the hydrological model, validation of the
427 model and the identification of vulnerable sub-basins by relating their flood peak and selected
428 indicators.
429

430 **4.1 Calibration and validation of the hydrological model**

Calibration is the iterative process to estimate the optimized basin parameters for satisfactory agreement between the simulated and observed data. But validation is a check that measures accuracy of a calibrated model, closed to the real independent forcing's. In the present study, the statistical parameters such as R^2, RMSE, and NSE were used as the performance criteria for the calibration and validation of the model.

4.1.1. Model calibration and its sensitivity

Automated method was adopted using the HEC-HMS model optimization technique (Feldman 2000) in order to calibrate the model. The model sensitivity (Fig.5a) towards the CN continues the calibration process by an adjustment of CN scaling factor with an objective to maximize the NSE. CN scaling factor is the fractional amount of change in the CN value. The surface runoff obtained from the calibrated model has direct relationship with the CN. The 0 CN value means that all the rain will infiltrate into the ground whereas 100 CN value means all the rainfall will flow as the surface runoff that signifies the ideal pavement condition. Ideally, the CN value cannot be greater than 98, since the surface will hold some little amount of rainfall (Halwatura and Najim 2013).

In this study, optimization trial run was implemented at the Sangam gauging station for the duration similar to model simulation run (Jun 2014 to Oct 2014), but the optimization objective run was scheduled daily for the event period during Sep 3, 2014 to Sep 15, 2014 against the daily observed available during that period only to derive the optimized CN scaling factor. Optimized CN scaling factor was then adjusted to derive the maximum NSE for the whole period of model simulation run (2014) to achieve the goal of calibration at the Sangam gauging station.

Fig.5a depicts sensitivity of the calibrated model with the maximum NSE value 0.989 obtained against the final optimized CN scaling factor, 0.98, governs the good efficiency of the model.

Correlation coefficient (R^2) of calibrated model obtained at the Sangam gauging station is 0.9935 (Fig.5c) signifies the good fit and the calibration curve between the observed and the simulated.

Fig.5. Calibration (2014) at Sangam: a) Model Sensitivity, b) Time Series, and c) Scattered plot

Fig.5c shows that the slope (0.9908) of the regression line at the Sangam is less than one has the minimal shift towards observed discharge with respect to the 45^0 line, signifying that the model is under predicting at Sangam. The calibrated peak flow simulated at the Sangam is 3425.90 m^3/s (Fig.5b) with -5.01 relative peak error percent. RMSE obtained for the calibrated model during the linear regression at the Sangam gauging station is 106.53 m^3/s. Calibrated outflow from the Sangam is now the inflow for the other stations such as RamMunshi Bagh and Asham in its downstream. CN of the sub-basins contributing to these two stations in the downstream are also optimized to obtain the good fit and calibration curves (Fig.6a and 6b) between the observed and the simulated at these sites. The maximum NSE obtained during this correlation process at the RamMunshi Bagh and Asham is 0.8437 and 0.7368. R^2 values 0.9588 and 0.9941 obtained during the correlation at RamMunshi Bagh and Asham, respectively shows the good fit curve. Model is over predicting at the RamMunshi Bagh and Asham since the shift in the regression line is towards the simulated one from the 45^0 line, having slopes (1.1481 and 1.2822) greater than 1. RMSE obtained at the RamMunshi Bagh and Asham during the whole process of regression is 187.75 m^3/s and 78.60 m^3/s.

Fig.6. Scattered plots (2014) at other stations: a) RamMunshi Bagh and b) Asham

4.1.2 Diversion and attenuation of the flood peak

This section enlightened the monitoring the capacity of reaches and the constructed Flood Spill Channel (FSC). However, FSC starts at Reduced Distance (RD) 68.64 km Jhelum River and FSC RD 0 km in between the Padshahi Bagh (RD 66.93 km Jhelum River) and RamMunshi Bagh (RD 71.70 km Jhelum River) gauging sites, respectively (Fig.2). While ends at the confluence point of FSC and Ferozpora (Kuzer branch) Nallah at FSC RD 32.62 km, respectively somewhere nearer to the downstream of Asham gauging site (RD 106.10 km), see Fig.2. The section also monitors the cause of attenuated peaks observed during the 2014 flood events, either it is due to diversion from FSC or due to the reduction in the capacity of FSC and reach or both. The diversion in peak discharge was also observed during the Jhelum 2014 flood from the (FSC) situated between the Padshahi Bagh (RD 66.93 km) and RamMunshi Bagh (71.70 km) gauging sites. According to Irrigation and flood control department, Kashmir the maximum observed diverted peak from the FSC was 244 m^3/s (8,600 cusec), 10.61% of peak at Padshahi Bagh (2299 cumec) gives the current capacity of the FSC during 2014 (Eptisa 2018; Romshoo et al. 2018). Diversion structure added between the Padshahi Bagh and RamMunshi Bagh in the configured calibrated model simulated the diverted peak flow as 223.16 cumec with relative percentage error 8.54 % at the same capacity of FSC observed during the 2014 flood. The details about the diversion from the FSC during the Jhelum 2014 flood are discussed in the Table 4. During 2014, with respect to the inflow from the Sangam (3262.61 Cumec), the maximum percentage of flow diverted from the FSC was also only 10.61% (244 Cumec) of Padshahi Bagh. Maximum diversion in the peak flow observed from the FSC with respect to the inflow from the Sangam (peak flow 1834.08 Cumec & 1780.44 Cumec) during the event years 1992 and 1997 were 36.81% & 45.17 %.

500 **Table 4:** Diversion of peak discharge during Jhelum 2014 flood

501

502 It was found that observed time lag (Fig.6.) in the peaks occurred at the gauging sites in the reach
503 during the Jhelum 2014 flood. Fig.6a. shows the approx. 11 hrs. (660 min) T_{lag} was observed at the
504 Sangam gauging location situated in the upstream of the Jhelum. Since, according to Central Water
505 Commission (CWC), the India Standard Time (IST) for starting the discharge data recording at the
506 gauging sites is 8:00 AM (CWC 2017), where 00:00 hrs. represent 12:00 AM. It was observed that
507 RamMunshi Bagh and Asham gauging sites have also T_{lag} 59 hrs. (2 days 11 hrs.), and 75 hrs. (3
508 days 3 hrs.), respectively with respect to the Sangam as depicted in the Fig.6b. T_{lag} at Asham
509 gauging station with respect to the RamMunshi Bagh was observed as 18 hrs. (108 min), see Fig.6b.
510 The reduction in the outflow peaks at the gauging locations, called attenuation (Subramanya 2008)
511 were also found in this study during the Jhelum 2014 flood event. Table 5 shows the attenuations
512 observed in the peaks at the respective gauging stations during 2014 flood event. Total 37.02% and
513 34.41% attenuation in the peaks of outflow at RamMunshi Bagh and Asham were found, with
514 respect to their respective recorded inflows in their upstream. The outflow at Asham has 58.61%
515 attenuation in its peak with respect to the inflow recorded at Sangam. Attenuation in the peak
516 discharge were also found in the observed flow during the event year 1992 at RamMunshi Bagh
517 and Asham by 36.81% and 0.55%, respectively with respect to the inflows from their respective
518 upstream reaches, where 1152.49 Cumec measured at Asham. During the year 1997, the attenuated
519 peak was also observed at both RamMunshi Bagh (976.13 Cumec, 45.17%) and Asham (824.30
520 Cumec, 15.55%).

521

522 **Fig.7.** a) Time lag (2014) at Sangam; b) flow (2014) at Sangam, RamMunshi Bagh & Asham

Table 5: Reach lag and attenuation in the outflow at the gauging stations during Jhelum 2014 flood

4.1.3. Model validation

The calibrated configured model is needed to be validated for checking the stability of the calibrated model (Halwatura and Najim 2013). In the current research, the model was validated at the Sangam gauging site (Sangam in the upstream has higher contribution percent in the flood peaks than RamMunshi Bagh and Asham in the downstream, see Fig.11 and Table 6 and 7) for the monsoon seasons of the years 1992 and 1997. Since during the monsoon period of selected validation years, the valley has also experienced the extreme flood events (Romshoo et al. 2018), see Fig.8. The statistical analysis of model validation results (see Fig.9) that manifest the good agreement of the calibrated model in predicting the real scenario in the studied basin. Correlation coefficient values obtained 0.9618 and 0.9486 exhibit good linear fitting of regression line during the years 1992 and 1997. Obtained slope values 0.9882 and 1.0210 for the years 1992 and 1997 show the shifting of regression line towards the observed and simulated, respectively. Also, the RMSE obtained for the regression analysis are 86.39 Cumec and 79.64 Cumec, respectively.

Fig.8. Year wise maximum flow at Sangam

Fig.9. Validation scattered plots at Sangam: a) year 1992 and b) year 1997

4.2 Flood vulnerability assessment of the sub-basins

545 The present section of the results and discussion highlights the vulnerable sub-basins that have
546 significant contribution to their flood peaks. The most dominant indicators of such sub-basins
547 influencing their flood peaks were also identified during the recognition process of these sub-basins
548 of the Jhelum River. The normalized scores of the basin characteristics and the VI score obtained
549 for each sub-basin are shown in Fig.10. It is observed that W810 (VI score - 0.645) and W950 (VI
550 score - 0.325) sub-basins are the most and the least vulnerable (Fig.12a and Table 6) sub-basins of
551 the Jhelum river contributing to the Sangam and RamMunshi Bagh gauging sites situated in the
552 upstream and downstream, respectively.
553
554 **Fig.10.** Sub-basins wise Vulnerability Index score plot with their classification using the color ramp
555 representation and the normalized score plot of their characteristics
556
557 **Fig.11.** D/S = Downstream (contributing to RamMunshi Bagh and Asham) and U/S = Upstream
558 (contributing to Sangam)
559
560 The sub-basins which has VI score below the obtained OTV 0.457, see Fig.11 were categorized as
561 highly vulnerable sub-basins that contributing significantly to their peak flood (Table 6). The OTV
562 for this classification was considered using the standard deviation classification method. Since,
563 among all the three adopted methods (mean, natural breaks, and standard deviation) for the OTV
564 selection, the standard deviation has minimum value and classify the maximum number sub-basins
565 of Jhelum river basin into the vulnerable category. All the highly vulnerable sub-basins of this
566 basin have benefaction to the Sangam gauging site situated in the upstream of the river except the
567 W610 which is contributing the Asham gauging station in the downstream the river. The most

568 influencing characteristics of such sub-basins belong to their respective gauging sites are discussed
569 in the Table 6. The hydrological characteristics (averaged normalized score – 0.844) have
570 dominated over the terrain, soil and LULC characteristics in case of most vulnerable sub-basin
571 W810. W810 has the lowest T_c (3.66 hrs.), highest LPA (1076.63 mm), low area (228.07 Km^2) and
572 high CN (76) comparison to the all other sub-basins signify its most vulnerable condition. Romshoo
573 et al. (2018) have also stated that the lower Tc and high slope gradients of sub-basins in the upstream
574 sides contributing to the Sangam are the indicators responsible for Jhelum 2014 flood event. The
575 lower T_c means the time required by the river flows to reach their respective junction will be very
576 low (Subramanya 2008). However, the dominant parameters of other highly vulnerable sub-basins
577 include the soil and terrain characteristics as well except LULC parameters. Fig.11 represents the
578 final map of the vulnerable sub-basins of Jhelum River stretched between maximum and minimum
579 VI scores 0.644 and 0.325, respectively depicts the high and the low vulnerable sub-basins.
580
581 **Table 6:** Sub-basins contributing significantly to the flood peak flows and their most dominant
582 influencing parameters
583
584 **Fig.12.** Vulnerability Index score map: a) sub-basins wise, and b) district wise
585
586 Fig.12b depicts the low and highly vulnerable sub-basins located in the respective districts.
587 Anantnag district has the largest area (2725.738 Km^2) amongst the all other districts covering
588 only the highly vulnerable sub-basins (100%) namely, W610, W700, W810, W1020, W1090, and
589 W1130, respectively (Table 7 and Fig.13), place it in the category of highly vulnerable. Like the
590 Anantnag district, Ganderbal, Kulgam and the part of Ramban are also 100% covering the only

591 highly vulnerable sub-basins as shown in the table 7 and Fig.13 made them highly vulnerable
592 districts. However, the Shupiyan district has both low (49.17 %) and highly (50.83%) vulnerable
593 sub-basins where the contribution of highly vulnerable is more that made the district highly
594 vulnerable. But, the VI score obtained for the district using the equation 9 as shown in Fig.13 has
595 made the Kulgam, the most vulnerable district and the Badgam as the least vulnerable. Badgam
596 and part of Baramulla have 100% contribution of only low vulnerable sub-basins however
597 Pulwama and Srinagar have both low and highly vulnerable sub-basins area covering where the
598 area percentage of low vulnerable sub-basins are high. The districts are also categorized into the
599 downstream (Badgam, part of Baramulla, Pulwama, Srinagar, and Ganderbal) and upstream
600 (Shupiyan, part of Ramban, Anantnag and Kulgam) parts, see Fig.13 based on the respective area
601 percentage of sub-basins (located in the upstream and downstream) in the districts for the easy
602 acquirement of information. Present study have used the indicator based approach for
603 vulnerability assessment using the indicators based on hydrological aspects of basin only.
604 However, the results may vary due to the use of only socio-economic indicators in this
605 vulnerability assessment. Hence, the integrated uses of hydrology and socio-economic based
606 indicators can be used for the future research in this field.
607
608 **Table 7:** Analysis of districts corresponds to the low and highly vulnerable sub-basins
609
610 **Fig.13.** Area contribution of sub-basins in the respective districts and district wise VI score
611
612 **5. Conclusion**

A novel approach using hydrological model and indicator-based GIS method for sub-basin level flood peak and vulnerability assessment has been proposed in this study.

1. The sub-basins W810 (Fig.2 and Fig.12b), part of Anantnag district, contributing to the Sangam gauging site, is found to be the most vulnerable among the all other sub-basins, see Fig.12a. The peak discharge of this basin was controlled by hydrological characteristics compared to other characteristics (e.g. terrain, soil; Table 6).
2. Various districts such as Shupiyan, Ganderbal, Anantnag, part of Rambana and Kulgam are falling under highly vulnerable category. However, Anantnag district (2725.738 Km^2) acquires the largest part of the highly vulnerable region of the Jhelum river basin, see Fig. 12b and Table 7.
3. It was found that 50% sub-basins falling in highly vulnerable category are contributing to the accumulated flow of Sangam station making upstream side of Jhelum River more vulnerable than the downstream side (Table 6 and 7).
4. Attenuation in the observed peak outflows were also observed during 2014 flood event due to reduction in the carrying capacity of river channel and FSC (Table 4 and 5). The overflow of discharge during that flood duration has caused the inundation in the regions surrounding to the Jhelum River. The flood inundation for that flooded period was mapped by Bhatt et al. (2017) using the Remote Sensing satellite data .The decrement in the capacity of the reach and the FSC were due the siltation and accumulation of sediments carried by the regular and the heavy flood flows.
5. These vulnerable sub-basins and the sub-basins with low Tc are needed to take care by the flood management authorities to prevent the region from such type of flood events in the future.

It is recommended to monitor the sediment flows along with the discharge on the regular basis in the channel and the FSC to avoid the 2014 flood events like situation in the future. Authorities should maintain (dredging for removing sediments) the existing FSCs and river channel regularly and increase the number of FSCs especially in the downstream of Sangam to increase the capacity of existing FSCs. In order to increase mitigation time during and before the extreme flood events, the increment in T_c of highly vulnerable sub-basins is advised through sustainable watershed management. It is recommended to use AI-based models and their hybrids in the future studies to improvise the results of hydrological predictions.

Acknowledgement

Our heartfelt thanks to Irrigation and flood control department, Kashmir and India Metrological Department for providing the discharge and rainfall data. We are also thankful to Director, Indian Institute of Remote Sensing, ISRO, Dehradun and Disaster Management Support (DMS) office of ISRO headquarters for their help, support and motivation during this entire research. This work was done as part of ISRO sponsored DMS (research and development) project "Remote sensing, ground observations and integrated modelling based early warning system for climatic extremes of North West Himalayan region."

Conflicts of interest/ Competing interest

The authors declare that they have no known competing financial interests or personal relationships that could have appeared to influence the work reported in this paper.

Availability of data and material

The data that support the findings of this study are available from the corresponding author Pankaj R. Dhote, upon reasonable request.

Code availability

Not applicable.

Authors' contributions

RR:Conceptualization, analysis and prepared original draft; PRD: Conceptualization, analysis and wrote paper; PKT: Reviewed paper and helped in producing figurers; SPA: Supervision and reviewed paper

References

Abdulkareem, J.H., Sulaiman, W.N.A., Pradhan, B., and Jamil, N.R., 2018. Relationship between design floods and land use land cover (LULC) changes in a tropical complex catchment. Arab J Geosci, 11 (14), 1–17. https://doi.org/10.1007/s12517-018-3702-4.

Abushandi, E. and Merkel, B., 2013. Modelling rainfall runoff relations using HEC-HMS and IHACRES for a single rain event in an arid region of Jordan. Water Resour Manage, 27(7), 2391-2409. https://doi.org/10.1007/s11269-013-0293-4..

Aggarwal S.P., Garg V., Thakur P.K., Nikam B.R., 2019. Hydrological Modelling in North Western Himalaya. In: Navalgund R., Kumar A., Nandy S. (eds). Remote Sensing of Northwest Himalayan Ecosystems. Springer, Singapore. https://doi.org/10.1007/978-981-13-2128-3_6.

Ahmad, T., Pandey, A.C., and Kumar, A., 2018a. Flood hazard vulnerability assessment in

681 Kashmir Valley , India using geospatial approach. Phy Chem Earth, Parts A/B/C, 105, 59–
682 71. https://doi.org/10.1016/j.pce.2018.02.003.
683
684 Álvarez, C., Juanes, J. a., García, A., Sainz, A., Puente, A., and Revilla, J. a., 2008. Surface
685 water resources assessment in scarcely gauged basins in the north of Spain. J
686 Hydrol, 356(3-4), 312-326. https://doi.org/10.1016/j.jhydrol.2008.04.019.
687 Ayalew, L., Yamagishi, H. and Ugawa, N., 2004. Landslide susceptibility mapping using GIS-
688 based weighted linear combination, the case in Tsugawa area of Agano River, Niigata
689 Prefecture, Japan. Landslides, 1(1), 73-81. https://doi.org/10.1007/s10346-003-0006-9.
690 Balasubramanian, A., Duraisamy, K., Thirumalaisamy, S., Krishnaraj, S., and Yatheendradasan,
691 R.K., 2017. Prioritization of subwatersheds based on quantitative morphometric analysis in
692 lower Bhavani basin, Tamil Nadu, India using DEM and GIS techniques. Arab J Geosci,
693 10 (24), 552. https://doi.org/10.1007/s12517-017-3312-6.
694 Behanzin, D.I., Thiel, M., Szarzynski, J., and Boko, M., 2016. GIS-Based Mapping of Flood
695 Vulnerability and Risk in the Bénin Niger River Valley. Int J Geomat Geosci, 6 (3), 1653–
696 1669.
697 Beyene, T., Lettenmaier, D.P., and Kabat, P., 2010. Hydrologic impacts of climate change on
698 the Nile River Basin: Implications of the 2007 IPCC scenarios. Climatic Change, 100 (3),
699 433–461. https://doi.org/10.1007/s10584-009-9693-0.
700 Bhat, M.S., Alam, A., Ahmad, B., Kotlia, B.S., Farooq, H., Taloor, A.K., and Ahmad, S., 2019.
701 Flood frequency analysis of river Jhelum in Kashmir basin. Quatern Int, 507, 288–294.
702 https://doi.org/10.1016/j.quaint.2018.09.039.
703 Bhatt, C.M., Rao, G.S., Farooq, M., Manjusree, P., Shukla, A., Sharma, S.V.S.P., Kulkarni,

S.S., Begum, A., Bhanumurthy, V., Diwakar, P.G., Dadhwal, V.K., Rao, G.S., Farooq, M., Manjusree, P., and Shukla, A., 2017. Satellite-based assessment of the catastrophic Jhelum floods of September 2014 , Jammu & Kashmir , India. Geomat Nat Haz Risk, 8 (2), 309–327. https://doi.org/10.1080/19475705.2016.1218943.

Bhattacharya, R.K., Chatterjee, N. Das, and Das, K., 2020. Sub-basin prioritization for assessment of soil erosion susceptibility in Kangsabati, a plateau basin: A comparison between MCDM and SWAT models. Sci Total Environ, 734, 139474. https://doi.org/10.1016/j.scitotenv.2020.139474.

Bhutiyani, M.R., Kale, V.S., and Pawar, N.J., 2010. Climate change and the precipitation variations in the northwestern Himalaya: 1866–2006. Int J Climatol*:* J R Meteorol Soc, 30 (4), 535–548. https://doi.org/10.1002/joc.1920.

Bilham, R., Bali, B.S., Bhat, M.I. and Hough, S., 2010. Historical earthquakes in Srinagar, Kashmir: Clues from the Shiva temple at Pandrethan. Ancient earthquakes, 471, 110-117.

Birkmann, J., 2006. Measuring vulnerability to promote disaster-resilient societies: Conceptual frameworks and definitions. Measuring vulnerability to natural hazards: Towards disaster resilient societies, 1(9), 3-7.

Biswas, B., Vignesh, K.S. and Ranjan, R., 2021. Landslide susceptibility mapping using integrated approach of multi-criteria and geospatial techniques at Nilgiris district of India. Arab J Geosci, 14(11), pp.1-17. https://doi.org/10.1007/s12517-021-07341-7.

Bobál, P., Podhorányi, M., Mudroň, I., and Holubec, M., 2015. Mathematical modelling of the dynamics of mountain basin snow cover in Moravian-Silesian Beskydy for operational purposes. Water Resour, 42 (3), 302–312. https://doi.org/10.1134/S0097807815030148.

Bosznay, M., 1989. Generalization of SCS curve number method. J Irrig Drain Eng, 115 (1),

139–144. https://doi.org/10.1061/(ASCE)0733-9437(1989)115:1(139).

Brody, S., Blessing, R., Sebastian, A., and Bedient, P., 2014. Examining the impact of land use/land cover characteristics on flood losses. J Environ Plan Manag , 57 (8), 1252–1265. https://doi.org/10.1080/09640568.2013.802228

Census of India, 2011 provisional population totals. New Delhi: Office of the Registrar General and Census Commissioner..

Chang, T.K., Talei, A., Alaghmand, S., and Ooi, M.P.L., 2017. Choice of rainfall inputs for event-based rainfall-runoff modeling in a catchment with multiple rainfall stations using data-driven techniques. J Hydrol, 545, 100–108. https://doi.org/10.1016/j.jhydrol.2016.12.024.

Chaponnière, A., Boulet, G., Chehbouni, A., and Aresmouk, M., 2008. Understanding hydrological processes with scarce data in a mountain environment. HydrolProcess, 22 (12), 1908–1921. https://doi.org/10.1002/hyp.6775.

Chen, H., Ito, Y., Sawamukai, M., and Tokunaga, T., 2015. Flood hazard assessment in the Kujukuri Plain of Chiba Prefecture, Japan, based on GIS and multicriteria decision analysis. Nat Haz, 78 (1), 105–120. https://doi.org/10.1007/s11069-015-1699-5.

Choudhary, H. and Badal, P.S., 2018. Assessing Climate Change Impacts and Vulnerability Indices in Regions of Eastern Uttar Pradesh. Indian J Eco Dev, 14 (1a), 18-22. http://dx.doi.org/10.5958/2322-0430.2018.00029.X.

Chouksey, A., Lambey, V., Nikam, B.R., Aggarwal, S.P. and Dutta, S., 2017. Hydrological modelling using a rainfall simulator over an experimental hillslope plot. Hydrology, 4(1), 17. https://doi.org/10.3390/hydrology4010017.

Chung, E.-S. and Lee, K.S., 2009. Prioritization of water management for sustainability using

hydrologic simulation model and multicriteria decision making techniques. J Environ Manage, 90 (3), 1502–1511. https://doi.org/10.1016/j.jenvman.2008.10.008.

Clark, G.E., Moser, S.C., Ratick, S.J., Dow, K., Meyer, W.B., Emani, S., Jin, W., Kasperson, J.X., Kasperson, R.E., and Schwarz, H.E., 1998. Assessing the vulnerability of coastal communities to extreme storms: the case of Revere, MA., USA. Mitigation and adaptation strategies for global change, 3 (1), 59–82.

Costache, R., Țîncu, R., Elkhrachy, I., Pham, Q.B., Popa, M.C., Diaconu, D.C., Avand, M., Costache, I., Arabameri, A., and Bui, D.T., 2020. New neural fuzzy-based machine learning ensemble for enhancing the prediction accuracy of flood susceptibility mapping. Hydrolog Sci J, 65 (16), 2816–2837. https://doi.org/10.1080/02626667.2020.1842412.

Cunge, J.A., 1969. On the subject of a flood propagation computation method (Musklngum method). J Hydraul Res, 7 (2), 205–230. https://doi.org/10.1080/00221686909500264.

Cutter, S.L., Boruff, B.J., and Shirley, W.L., 2003. Social vulnerability to environmental hazards. Social science quarterly, 84 (2), 242–261.

CWC. 2017. Handbook for Hydrometeorological Observations. Ministry of Water Resources, River Development and Ganga Rejuvenation, Government of India. http://www.cwc.gov.in/sites/default/files/final-hm-handbook-jan-2017.pdf.

.

D'Asaro, F. and Grillone, G., 2012. Empirical investigation of curve number method parameters in the Mediterranean area. J Hydrol Eng, 17 (10), 1141–1152. https://doi.org/10.1061/(ASCE)HE.1943-5584.0000570.

Dar, R.A., Chandra, R., Romshoo, S.A., Lone, M.A., and Ahmad, S.M., 2015. Isotopic and micromorphological studies of Late Quaternary loess–paleosol sequences of the Karewa

Group: inferences for palaeoclimate of Kashmir Valley. Quatern Int, 371, 122–134. https://doi.org/10.1016/j.quaint.2014.10.060.

Dhar, O.N., Mandal, B.N., and Kulkarni, A.K., 1982. Effect of the Pir Panjal range of Himalayas over monsoon rainfall distribution in Kashmir Valley. In: Proc. Int. Symp. hydrological aspects of mountainous watersheds.

Dhar, O.N. and Nandargi, S., 2003. Hydrometeorological aspects of floods in India. Nat Haz, 28 (1), 1–33. https://doi.org/10.1023/A:1021199714487.

Dhar, O.N. and Nandargi, S., 2005. Distribution of precipitation over the Himalayas. J Met, 30, 83–91.

Dhote, P. R., Thakur, P. K., Aggarwal, S. P., Sharma, V. C., Garg, V., Nikam, B. R., and Chouksey, A., 2018. Experimental Flood Early Warning System In Parts of Beas Basin Using Integration of Weather Forecasting, Hydrological and Hydrodynamic Models. Int Arch Photogramm Remote Sens Spatial Inf Sci, XLII-5, 221–225. https://doi.org/10.5194/isprs-archives-XLII-5-221-2018.

Dhote, P.R., Aggarwal, S.P., Thakur, P.K. and Garg, Vaibhav, 2019. Flood inundation prediction for extreme flood events: a case study of Tirthan River, North West Himalaya. Himal Geol, 40(2), 128-140.Ebi, K.L., Woodruff, R., Von Hildebrand, A., and Corvalan, C., 2007. Climate change-related health impacts in the Hindu Kush-Himalayas. EcoHealth, 4 (3), 264–270. https://doi.org/10.1007/s10393-007-0119-z.

Engineers, U.S. Army Corps, 2008. Hydrologic modeling system (HEC-HMS) application guide: version 3.1. 0. Institute for Water Resources, Davis.

Eptisa, 2018. Jhelum and Tawi Flood Recovery Project. The World Bank. http://jtfrp.in/wp-content/uploads/2019/03/Task1_Report_Final.pdf.

ESRI, 2011. Release 10.2.1. Redlands, CA: Environmental Systems Research Institute.

Falah, F., Rahmati, O., Rostami, M., Ahmadisharaf, E., Daliakopoulos, I.N., and Pourghasemi, H.R., 2019. Artificial Neural Networks for Flood Susceptibility Mapping in Data-Scarce Urban Areas. Spatial Model in GIS and R for Earth Environ Sci (323-336). Elsevier Inc. https://doi.org/10.1016/B978-0-12-815226-3.00014-4.

Feldman, A.D., 2000a. Hydrologic Modeling System HEC-HMS technical reference manual: US Army Corps of Engineers. Hydrologic Engineering Center (609 Second St., Davis, CA 95616).

Feldman, A.D., 2000b. Hydrologic modeling system HEC-HMS: technical reference manual. US Army Corps of Engineers, Hydrologic Engineering Center.

Ganjoo, R.K., 2014. The Vale of Kashmir: Landform Evolution and Processes BT- Landscapes and Landforms of India. In: Kale V. (eds) Landscapes and Landforms of India. World Geomorphological Landscapes, , 125–133. Springer, Dordrecht. https://doi.org/10.1007/978-94-017-8029-2_11.

Ganju, A. and Dimri, A.P., 2004. Prevention and Mitigation of Avalanche Disasters in Western Himalayan Region. NatHaz, 31 (2), 357–371. https://doi.org/10.1023/B:NHAZ.0000023357.37850.aa.

Garg, V., Aggarwal, S.P., Gupta, P.K., Nikam, B.R., Thakur, P.K., Srivastav, S.K. and Kumar, A.S., 2017. Assessment of land use land cover change impact on hydrological regime of a basin. Environ Earth Sci, 76(18), 1-17. https://doi.org/10.1007/s12665-017-6976-z.

Gebre, S.L., 2015. Application of the HEC-HMS Model for Runoff Simulation of Upper Blue Nile River Basin. Hydrol: Current Res, 6 (2), 1.

Halwatura, D. and Najim, M.M.M., 2013. Application of the HEC-HMS model for runoff

simulation in a tropical catchment. Environ Modell Softw, 46, 155–162. https://doi.org/10.1016/j.envsoft.2013.03.006.

Hari, K., Durga, V., Rao, V.V., and Dadhwal, V.K., 2011. A Distributed Model for Real-Time Flood Forecasting in the Godavari Basin Using Space Inputs. Int J Disaster Risk Sci, 2 (3), 31–40. https://doi.org/10.1007/s13753-011-0014-7.

He, Z., Wen, X., Liu, H., and Du, J., 2014. A comparative study of artificial neural network, adaptive neuro fuzzy inference system and support vector machine for forecasting river flow in the semiarid mountain region. J Hydrol, 509, 379–386. https://doi.org/10.1016/j.jhydrol.2013.11.054.

Hong, H., Panahi, M., Shirzadi, A., Ma, T., Liu, J., Zhu, A.X., Chen, W., Kougias, I., and Kazakis, N., 2018. Flood susceptibility assessment in Hengfeng area coupling adaptive neuro-fuzzy inference system with genetic algorithm and differential evolution. Sci Total Environ, 621, 1124–1141. https://doi.org/10.1016/j.scitotenv.2017.10.114.

Huang, L., Liu, X., Liu, Y., Lang, B., and Tao, D., 2017. Centered weight normalization in accelerating training of deep neural networks. In: Proceedings of the IEEE International Conference on Computer Vision. 2803–2811.

Hunukumbura, P.B., Weerakoon, S.B. and Herath, S., 2008. Runoff modeling in the upper Kotmale Basin. Traversing No Man's Land, Interdisciplinary Essays in Honor of Professor Madduma Bandara. University of Peradeniya, Sri Lanka, 169-184. Ibrahim-Bathis, K. and Ahmed, S.A., 2016. Rainfall-runoff modelling of Doddahalla watershed—an application of HEC-HMS and SCN-CN in ungauged agricultural watershed. Arab J Geosci, 9 (3), 170. https://doi.org/10.1007/s12517-015-2228-2.

Ives, J.D., 2004. Himalayan Perceptions: Environmental change and the well-being of mountain

peoples(Vol. 6). Routledge, Taylor and Francis Group.

Jaafar, H.H., Ahmad, F.A., and El Beyrouthy, N., 2019. GCN250, new global gridded curve numbers for hydrologic modeling and design. Sci Data, 6 (1), 1–9. https://doi.org/10.1038/s41597-019-0155-x.

Jenks, G.F., 1967. The data model concept in statistical mapping. International yearbook of cartography, 7, 186–190.

Jenson, S.K. and Domingue, J.O., 1988. Extracting topographic structure from digital elevation data for geographic information system analysis. Photogrammetric engineering and remote sensing, 54 (11), 1593–1600.

Jonkman, S.N., 2005. Global perspectives on loss of human life caused by floods. Nat Haz, 34 (2), 151–175. https://doi.org/10.1007/s11069-004-8891-3.

Keshari, A.K., Satapathy, D.P. and Kumar, A., 2010. The influence of vertical density and velocity distributions on snow avalanche runout. Annals of glaciology, 51(54), 200-206. https://doi.org/10.3189/172756410791386409.

Kim, N.W. and Lee, J., 2008. Temporally weighted average curve number method for daily runoff simulation. Hydrol Process: IntJ, 22 (25), 4936–4948. https://doi.org/10.1002/hyp.7116.

Koneti, S., Sunkara, S.L., and Roy, P.S., 2018. Hydrological Modeling with Respect to Impact of Land-Use and Land-Cover Change on the Runoff Dynamics in Godavari River Basin Using the HEC-HMS Model. ISPRS Int J of Geo-Inf, 7(6), 206. https://doi.org/10.3390/ijgi7060206.

Kumar, R. and Acharya, P., 2016. Flood hazard and risk assessment of 2014 floods in Kashmir Valley : a space-based multisensor approach. Nat Haz, 84 (1), 437–464.

https://doi.org/10.1007/s11069-016-2428-4.

Kumar, S., Raizada, A., Biswas, H., Srinivas, S., and Mondal, B., 2016. Assessment of vulnerability to climate change: A case study of Karnataka. Indian J of Soil Conservation, 44 (3), 314–320.

Lawrence, S.W.R., 1895. The Valley of Kashmir. Asian Education Services, New Delhi.

Li, Y., Grimaldi, S., Walker, J.P., and Pauwels, V.R.N., 2016. Application of remote sensing data to constrain operational rainfall-driven flood forecasting: A review. Remote Sensing, 8 (6), 456. https://doi.org/10.3390/rs8060456.

Loukas, A. and Vasiliades, L., 2014. Streamflow simulation methods for ungauged and poorly gauged watersheds. Nat Haz Earth Syst Sci, 14 (7), 1641–1661. https://doi.org/10.5194/nhess-14-1641-2014.

Maqsood, S.T., Schwarz, J., 2010. Comparison of Seismic Vulnerability of Buildings before and after 2005 Kashmir Earthquake. Seismological Research Letters, 81 (1), 85–98. https://doi.org/10.1785/gssrl.81.1.85.

Mehdizadeh, S., Fathian, F., and Adamowski, J.F., 2019. Hybrid artificial intelligence-time series models for monthly streamflow modeling. Applied Soft Computing, 80, 873–887. https://doi.org/10.1016/j.asoc.2019.03.046.

Meraj, G., Romshoo, S.A., R. Yousuf, A., Altaf, S., and Altaf, F., 2015. Assessing the influence of watershed characteristics on the flood vulnerability of Jhelum basin in Kashmir Himalaya. Nat Haz, 77(1), 153-175. https://doi.org/10.1007/s11069-015-1605-1.

Milewski, A., Sultan, M., Yan, E., Becker, R., Abdeldayem, A., Soliman, F., and Gelil, K.A., 2009. A remote sensing solution for estimating runoff and recharge in arid environments. J Hydrol, 373 (1–2), 1–14. https://doi.org/10.1016/j.jhydrol.2009.04.002.

Mishra, A. and Srinivasan, J., 2013. Did a cloud burst occur in Kedarnath during 16 and 17 June 2013? Current Science, 105 (10), 1351–1352.

Mishra, S.K., Jain, M.K., and Singh, V.P., 2004. Evaluation of the SCS-CN-based model incorporating antecedent moisture. Water Resour Manag, 18 (6), 567–589. https://doi.org/10.1007/s11269-004-8765-1.

Miyato, T., Kataoka, T., Koyama, M., and Yoshida, Y., 2018. Spectral normalization for generative adversarial networks. arXiv preprint arXiv:1802.05957.

Mousavi, S.M. and Rostamzadeh, H., 2019. Estimation of flood land use/land cover mapping by regional modelling of flood hazard at sub-basin level case study: Marand basin. Geomat Nat Haz Risk, 10(1), 1155-1175. https://doi.org/10.1080/19475705.2018.1549112.

Morid, S., Gosain, A.K. and Keshari, A.K., 2002, July. Comparison of the SWAT model and ANN for daily simulation of runoff in snowbound ungauged catchments. In Fifth international conference on hydroinformatics, Cardiff, UK.

Murari, L., Nozawa, T., Emori, S., Harasawa, H., Takahashi, K., Kimoto, M., Abe-Ouchi, A., Nakajima, T., Takemura, T., and Numaguti, A., 2001. Future climate change: Implications for Indian summer monsoon and its variability. Current Science, 81 (9), 1196–1207.

Nandargi, S. and Dhar, O.N., 2011. Extreme rainfall events over the Himalayas between 1871 and 2007. Hydrolog Sci J, 56 (6), 930–945. https://doi.org/10.1080/02626667.2011.595373.

Nasiri, H., Yusof, M.J.M., and Ali, T.A.M., 2016. An overview to flood vulnerability assessment methods. Sustain Water Resour Manag 2 (3), 331–336. https://doi.org/10.1007/s40899-016-0051-x.

Nikam, B.R., Garg, V., Jeyaprakash, K., Gupta, P.K., Srivastav, S.K., Thakur, P.K. and

Aggarwal, S.P., 2018. Analyzing future water availability and hydrological extremes in the Krishna basin under changing climatic conditions. Arab J Geosci, 11(19), 1-16. https://doi.org/10.1007/s12517-018-3936-1.

Nourani, V., Kisi, Ö., and Komasi, M., 2011. Two hybrid artificial intelligence approaches for modeling rainfall–runoff process. J Hydrol, 402 (1–2), 41–59. https://doi.org/10.1016/j.jhydrol.2011.03.002.

NRCS, U., 1986. Urban Hydrology for Small Watersheds (TR-55). Engineering Division, Soil Conservation Service, US Department of Agriculture.

Parry, M., Parry, M.L., Canziani, O., Palutikof, J., Van der Linden, P. and Hanson, C. eds., 2007. Climate change 2007-impacts, adaptation and vulnerability: Working group II contribution to the fourth assessment report of the IPCC (Vol. 4). Cambridge University Press.Planning Commission, 2011. Report of working group on flood management and region specific issues for XII plan. Govt of India, New Delhi. Ponce, V.M., 1994. Engineering Hydrology: Principles and Practices (Vol. 640). Englewood Cliffs, N.J. : Prentice Hall.

Prakash, S. and Abhisek, M., 2016. Flash flood risk assessment for upper Teesta river basin : using the hydrological modeling system (HEC-HMS) software. Model Earth Syst Environ, 2 (2), 59. https://doi.org/10.1007/s40808-016-0110-1.

Rahadianto, H., Fariza, A. and Hasim, J.A.N., 2015, November. Risk-level assessment system on Bengawan Solo River basin flood prone areas using analytic hierarchy process and natural breaks: Study case: East Java. In 2015 International Conference on Data and Software Engineering (ICoDSE) (195-200). IEEE. https://doi.org/10.1109/ICODSE.2015.7436997.

934 Ray, P.K.C., Parvaiz, I., Jayangondaperumal, R., Thakur, V.C., Dadhwal, V.K., and Bhat, F.A.,
935 2009. Analysis of seismicity-induced landslides due to the 8 October 2005 earthquake in
936 Kashmir Himalaya. Current Science, 97 (12), 1742–1751.
937 Razmkhah, H., Saghafian, B., Ali, A.-M.A., and Radmanesh, F., 2016a. Rainfall-runoff
938 modeling considering soil moisture accounting algorithm, case study: Karoon III River
939 basin. Water Resou*r*, 43 (4), 699–710. https://doi.org/10.1134/S0097807816040072.
940 Razmkhah, H., 2016b. Comparing performance of different loss methods in rainfall-runoff
941 modeling. Water Resour, 43 (1), 207–224. https://doi.org/10.1134/S0097807816120058.
942 Reshma, T., Kumar, P.S., Babu, M.J.R.K., and Kumar, K.S., 2010. Simulation of runoff in
943 watersheds using SCS-CN and muskingum-cunge methods using remote sensing and
944 geographical information systems. Int J Adv SciTech, 25 (31).
945 Romshoo, S.A., Altaf, S., Rashid, I., and Ahmad Dar, R., 2018. Climatic, geomorphic and
946 anthropogenic drivers of the 2014 extreme flooding in the Jhelum basin of Kashmir, India.
947 Geomat Nat Haz Risk, 9 (1), 224–248. https://doi.org/10.1080/19475705.2017.1417332.
948 Romshoo, S.A., Bhat, S.A., and Rashid, I., 2012. Geoinformatics for assessing the
949 morphometric control on hydrological response at watershed scale in the upper Indus
950 Basin. J Earth Syst Sci, 121 (3), 659–686. https://doi.org/10.1007/s12040-012-0192-8.
951 Sadek, M., Li, X., Mostafa, E., Freeshah, M., Kamal, A., Sidi Almouctar, M.A., Zhao, F. and
952 Mustafa, E.K., 2020. Low-cost solutions for assessment of flash flood impacts using
953 Sentinel-1/2 data fusion and hydrologic/hydraulic modeling: Wadi El-Natrun Region,
954 Egypt. Advances in Civil Engineering, 2020. https://doi.org/10.1155/2020/1039309.
955 Sanyal, J., Densmore, A.L., and Carbonneau, P., 2014. Analysing the effect of land-
956 use/cover changes at sub-catchment levels on downstream flood peaks: A semi-distributed

957 modelling approach with sparse data. Catena, 118, 28–40.
958 https://doi.org/10.1016/j.catena.2014.01.015.
959 Scharffenberg, W.A. and Fleming, M.J., 2006. Hydrologic modeling system HEC-HMS: user's
960 manual. US Army Corps of Engineers, Hydrologic Engineering Center.
961 Schwab, G.O., Fangmeier, D.D., Elliot, W.J., and Frevert, R.K., 2005. Soil and Water
962 Conservation Engineering. fourth. New york: Jhon Wiley and Sons.
963 Shamseldin, A.Y., O'Connor, K.M., and Nasr, A.E., 2007. A comparative study of three neural
964 network forecast combination methods for simulated river flows of different rainfall-runoff
965 models. Hydrolog Sci J, 52 (5), 896–916. https://doi.org/10.1623/hysj.52.5.896.
966 Sikka, D.R., 1999. Influence of Himalayas and snow cover on the weather and climate of India-
967 A review. The Himalayan Environment, 37–52.
968 Singh, O. and Kumar, M., 2013. Flood events, fatalities and damages in India from 1978 to
969 2006. Nat Haz, 69 (3), 1815–1834. https://doi.org/10.1007/s11069-013-0781-0.
970 Singh, S., Dhote, P.R., Thakur, P.K., Chouksey, A., and Aggarwal, S.P., 2020. Identification of
971 flash-floods-prone river reaches in Beas river basin using GIS-based multi-criteria
972 technique: validation using field and satellite observations. Nat Haz, 105 (3), 2431–2453.
973 https://doi.org/10.1007/s11069-020-04406-w.
974 Soulis, K.X. and Valiantzas, J.D., 2012. SCS-CN parameter determination using rainfall-runoff
975 data in heterogeneous watersheds – the two-CN system approach. Hydrol Earth Syst Sci
976 16(3), 1001–1015. https://doi.org/10.5194/hess-16-1001-2012.
977 Stefanidis, S. and Stathis, D., 2013. Assessment of flood hazard based on natural and
978 anthropogenic factors using analytic hierarchy process (AHP). Nat Haz, 68 (2), 569–585.
979 https://doi.org/10.1007/s11069-013-0639-5.

Stewart, D., Canfield, E., and Hawkins, R., 2012. Curve number determination methods and uncertainty in hydrologic soil groups from semiarid watershed data. J Hydrol Eng, 17 (11), 1180–1187. https://doi.org/10.1061/(ASCE)HE.1943-5584.0000452.

Subramanya, K., 2008. Engineering Hydrology. Third. New Delhi: Tata McGraw-Hill Publishing Company Limited.

Sun, J., Cao, X., Liang, H., Huang, W., Chen, Z. and Li, Z., 2020, April. New interpretations of normalization methods in deep learning. In Proceedings of the AAAI Conference on Artificial Intelligence (Vol. 34, No. 04, pp. 5875-5882). Talei, A. and Chua, L.H.C., 2012. Influence of lag time on event-based rainfall–runoff modeling using the data driven approach. J Hydrol, 438, 223–233. https://doi.org/10.1016/j.jhydrol.2012.03.027.

Tang, Q., Schilling, O.S., Kurtz, W., Brunner, P., Vereecken, H., and Hendricks Franssen, H., 2018. Simulating Flood-Induced Riverbed Transience Using Unmanned Aerial Vehicles, Physically Based Hydrological Modeling, and the Ensemble Kalman Filter. Water Resour Res, 54 (11), 9342–9363. https://doi.org/10.1029/2018WR023067.

Termeh, Seyed Vahid Razavi, Aiding Kornejady, Hamid Reza Pourghasemi, and Saskia Keesstra, 2018. Flood susceptibility mapping using novel ensembles of adaptive neuro fuzzy inference system and metaheuristic algorithms. Sci Total Environ 615, 438-451. https://doi.org/10.1016/j.scitotenv.2017.09.262.

Thakur P. K., Aggarwal, S. P., Dhote P., Nikam, B. R., Garg, V., Bhatt, C. M., Chouksey, A. and Jha, A., 2019. Hydrometeorological Hazards Mapping, Monitoring and Modelling. In: Navalgund R., Kumar A., Nandy S. (eds.) Remote Sensing of Northwest Himalayan Ecosystems, eBook ISBN:978-981-13-2128-3. Springer Singapore. https://doi.org/10.1007/978-981-13-2128-3.

1003 Thakur, P. K., Ranjan, R., Singh, S., Dhote, P. R., Sharma, V., Srivastav, V., Dhasmana, M.,
1004 Aggarwal, S. P., Chauhan, P., Nikam, B. R., Garg, V., and Chouksey, A., 2020. Synergistic
1005 Use of Remote Sensing, Gis And Hydrological Models for Study of August 2018 Kerala
1006 Floods. Int Arch Photogramm Remote Sens Spatial Inf Sci, XLIII-B3-2020, 1263–1270,
1007 https://doi.org/10.5194/isprs-archives-XLIII-B3-2020-1263-2020.
1008 Vignesh, K.S., Anandakumar, I., Ranjan, R., and Borah, D., 2020. Flood vulnerability
1009 assessment using an integrated approach of multi-criteria decision-making model and
1010 geospatial techniques. Model Earth Syst Environ , 7(2), 767-781.
1011 https://doi.org/10.1007/s40808-020-00997-2.
1012 Watson, R.T. and Haeberli, W., 2004. Environmental threats, mitigation strategies and high-
1013 mountain areas. AMBIO: J Human Environ, *33*(sp13), 2-10. https://doi.org/10.1007/0044-
1014 7447-33.sp13.2. Wu, S.-Y., Yarnal, B., and Fisher, A., 2002. Vulnerability of coastal
1015 communities to sea-level rise: a case study of Cape May County, New Jersey, USA.
1016 Climate research, 22 (3), 255–270. https://doi.org/10.3354/cr022255.
1017 Xiao, Y., Yi, S., and Tang, Z., 2017. Integrated flood hazard assessment based on spatial
1018 ordered weighted averaging method considering spatial heterogeneity of risk preference.
1019 Sci Total Environ, 599, 1034–1046. https://doi.org/10.1016/j.scitotenv.2017.04.218.
1020 Xs, H.R., Ross-larson, B., De Coquereaumont, M., Trott, C., Watkins, K., Carvajal, L., Ghosh,
1021 A., and Johansson, C., 2006. Human development report 2006.
1022 Yalcin, E., 2020. Assessing the impact of topography and land cover data resolutions on two-
1023 dimensional HEC-RAS hydrodynamic model simulations for urban flood hazard analysis.
1024 Nat Haz, 101 (3), 995–1017. https://doi.org/10.1007/s11069-020-03906-z.
1025 Yan, K., Di Baldassarre, G., Solomatine, D.P., and Schumann, G.J., 2015. A review of low-cost

space-borne data for flood modelling: topography, flood extent and water level. Hydrol Process, 29 (15), 3368–3387. https://doi.org/10.1002/hyp.10449.

Yoon, D.K., 2012. Assessment of social vulnerability to natural disasters: A comparative study. Nat Haz, 63 (2), 823–843. https://doi.org/10.1007/s11069-012-0189-2.

Young, C.C. and Liu, W.C., 2015. Prediction and modelling of rainfall–runoff during typhoon events using a physically-based and artificial neural network hybrid model. Hydrological Sciences Journal, 60 (12), 2102–2116. https://doi.org/10.1080/02626667.2014.959446.

Žurovec, O., Čadro, S., and Sitaula, B.K., 2017. Quantitative assessment of vulnerability to climate change in rural municipalities of Bosnia and Herzegovina. Sustainability*)*, 9 (7), 1208. https://doi.org/10.3390/su9071208.

Figures

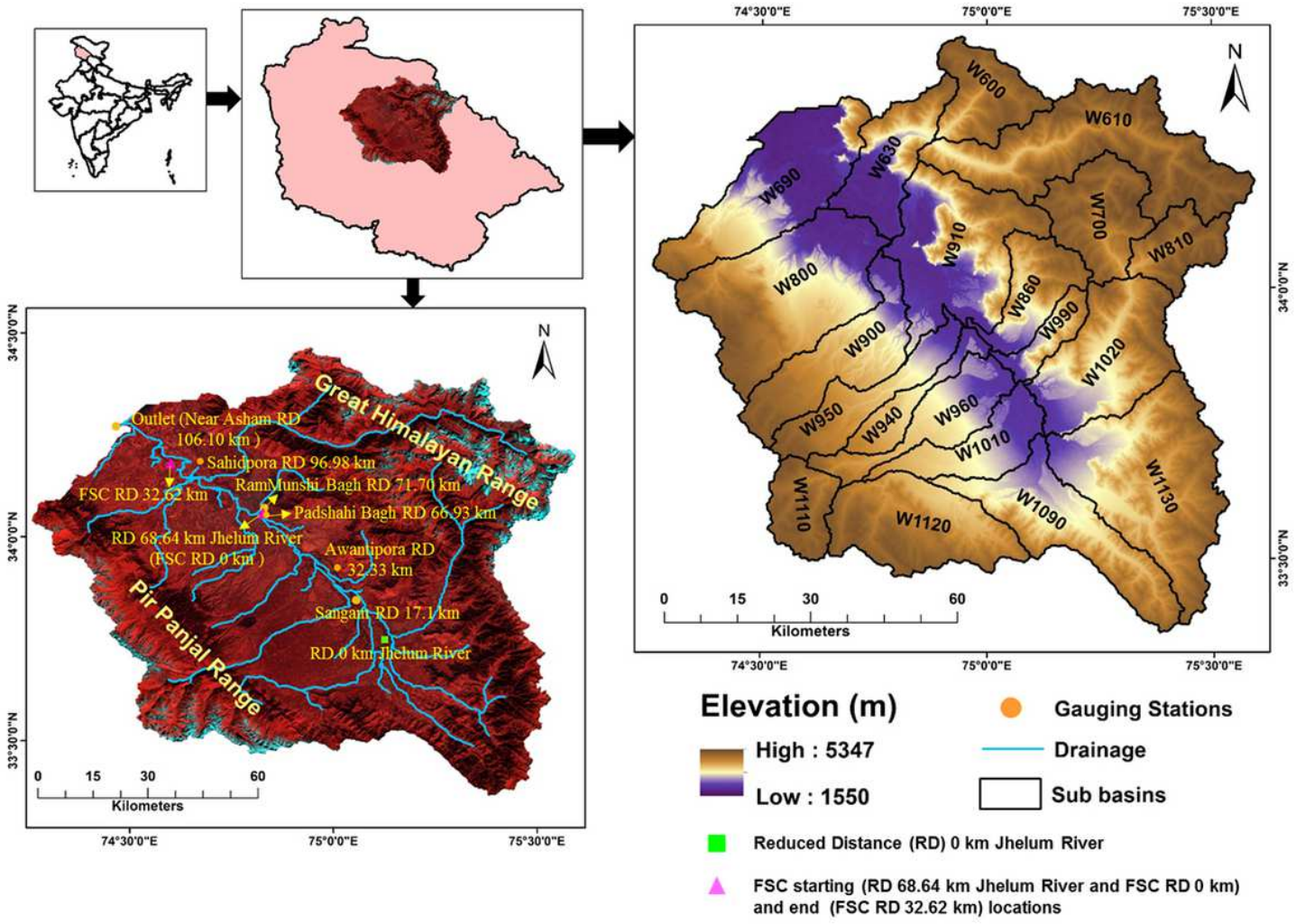

Figure 1

Jhelum River basin with outlet, drainages, sub-basins & gauging sites

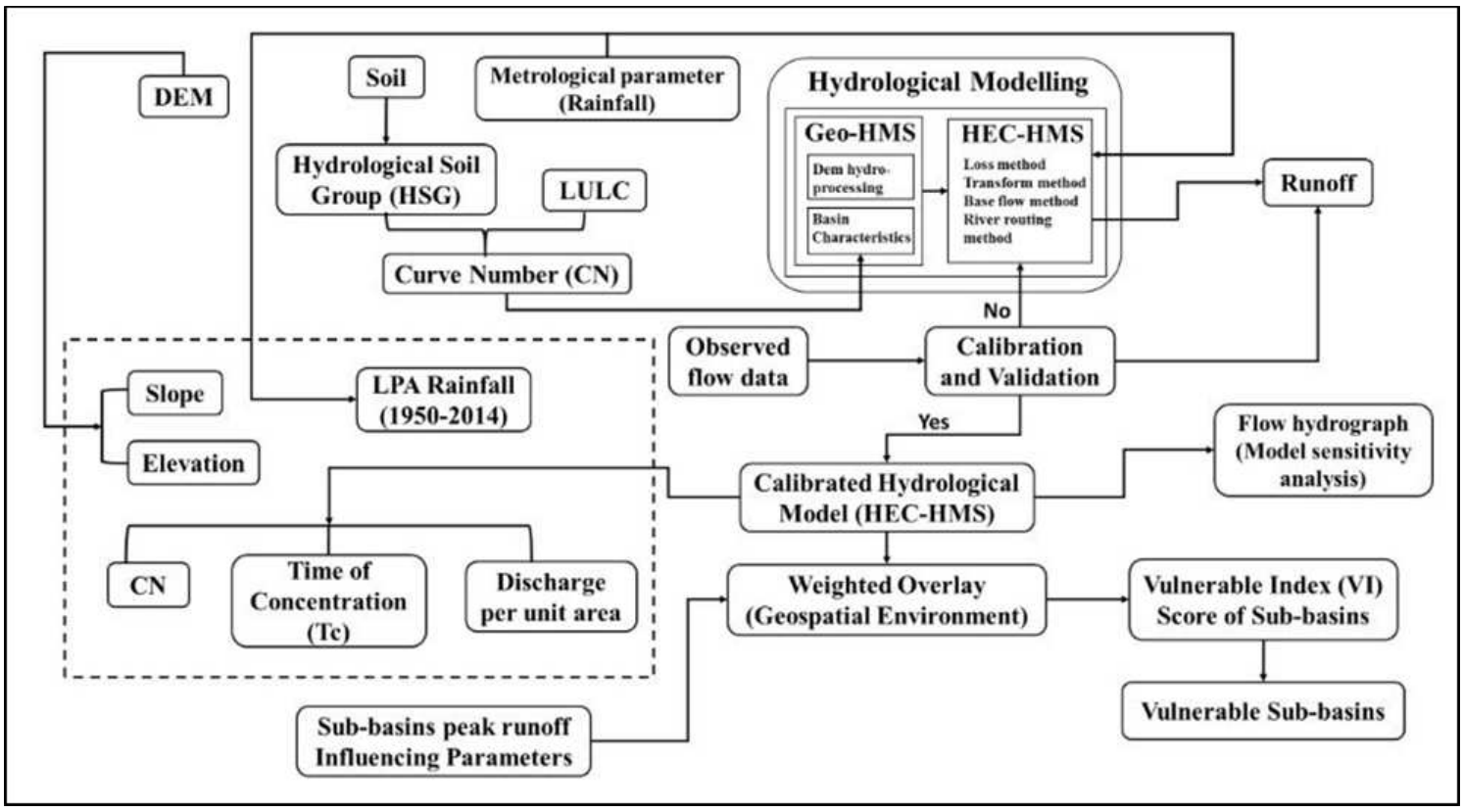

Figure 2

Methodology flowchart

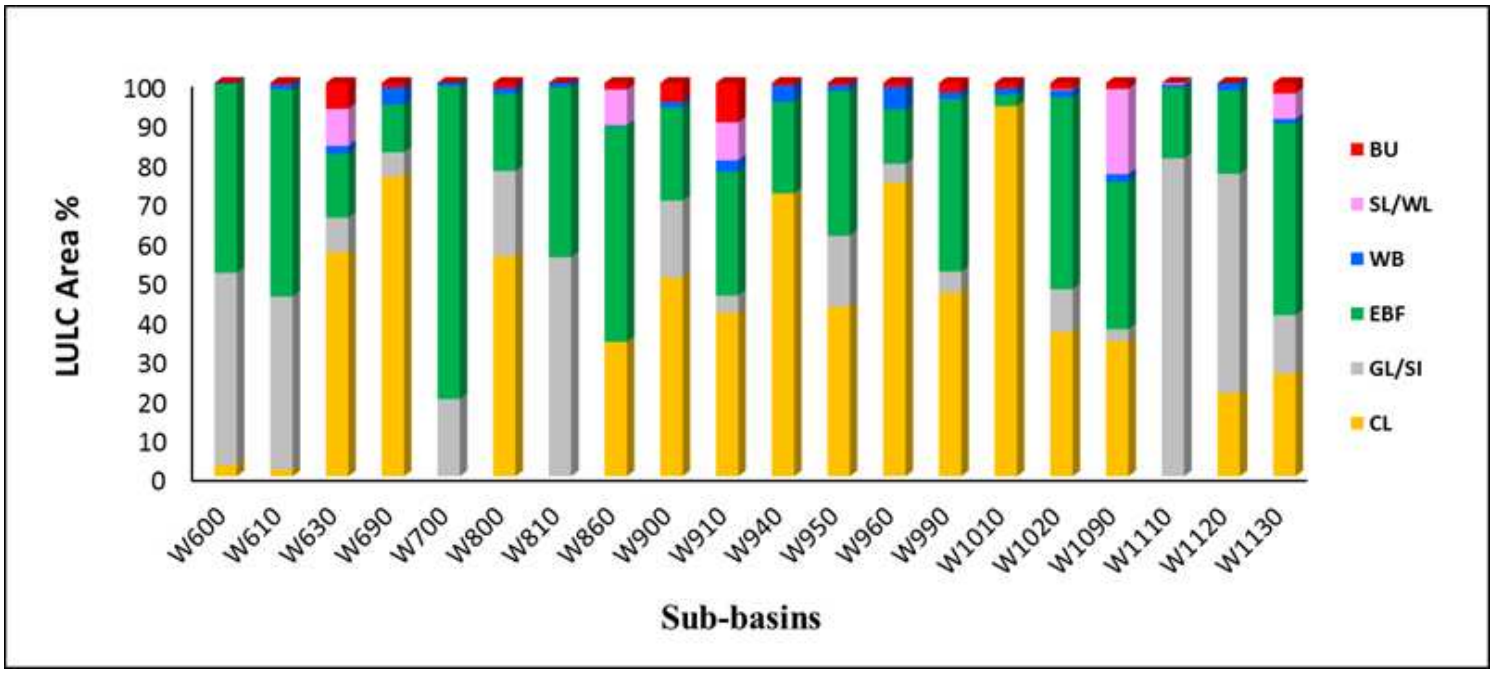

Figure 3

LULC percent of each sub-basin

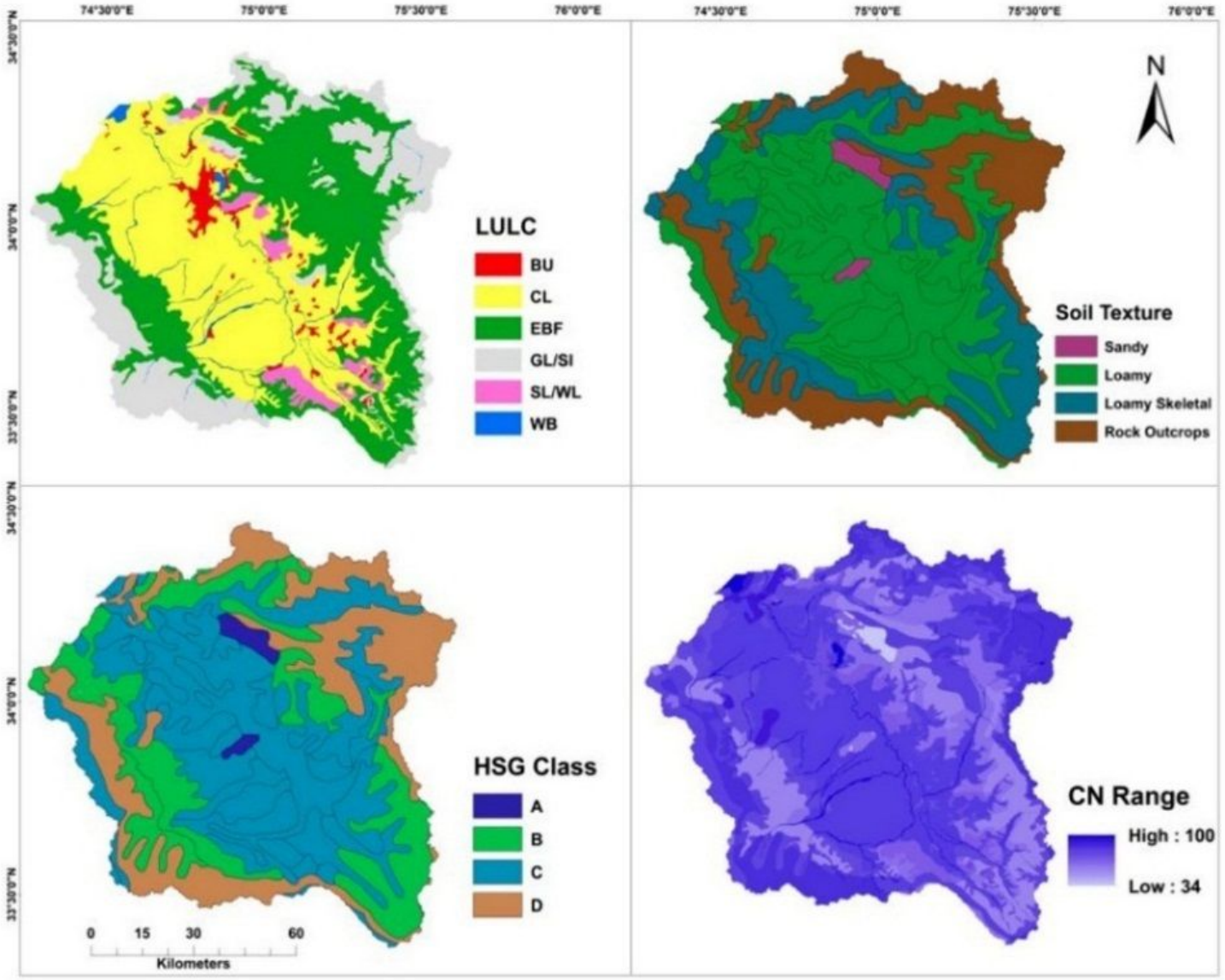

Figure 4

LULC, Soil, HSG and CN Map of Jhelum basin

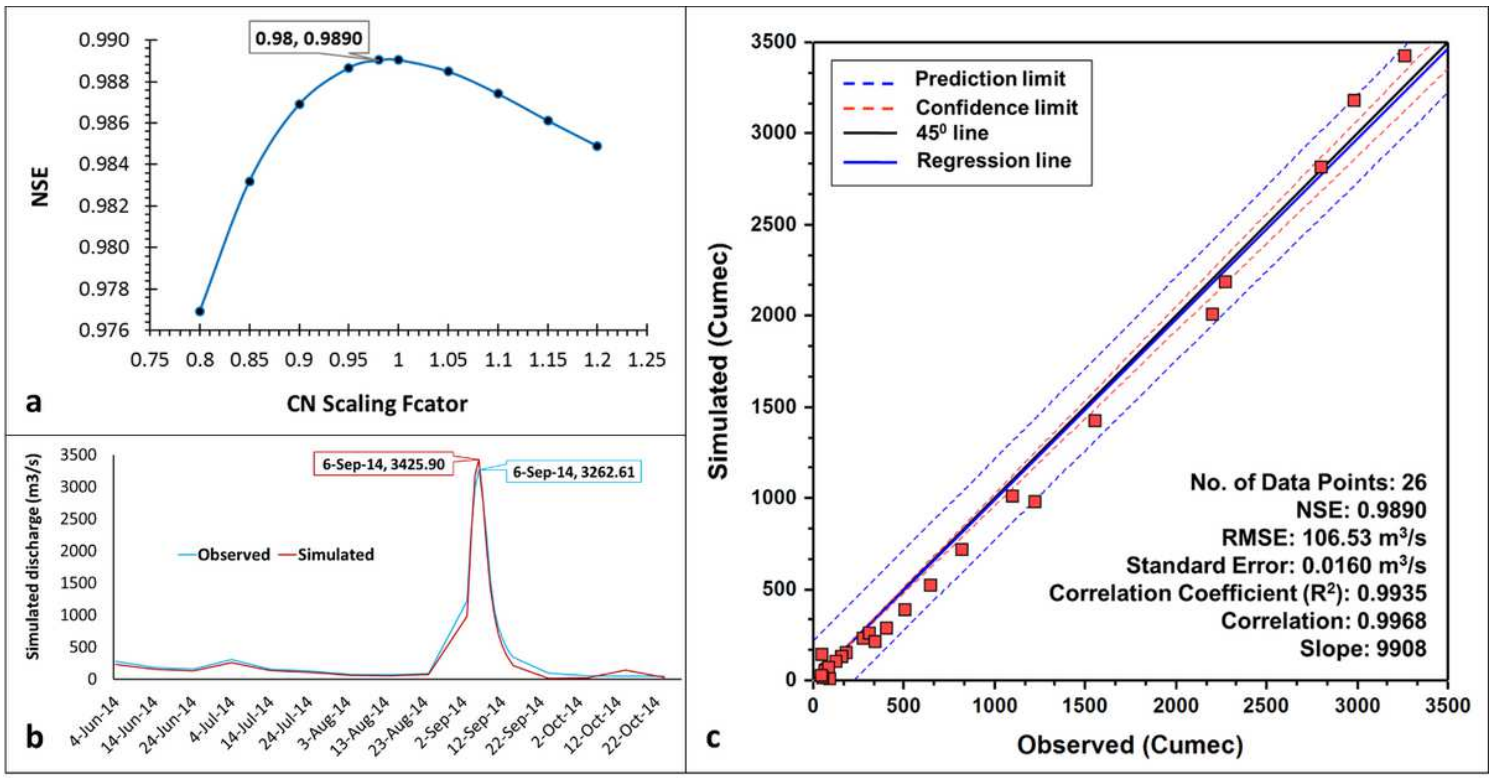

Figure 5

Calibration (2014) at Sangam: a) Model Sensitivity, b) Time Series, and c) Scattered plot

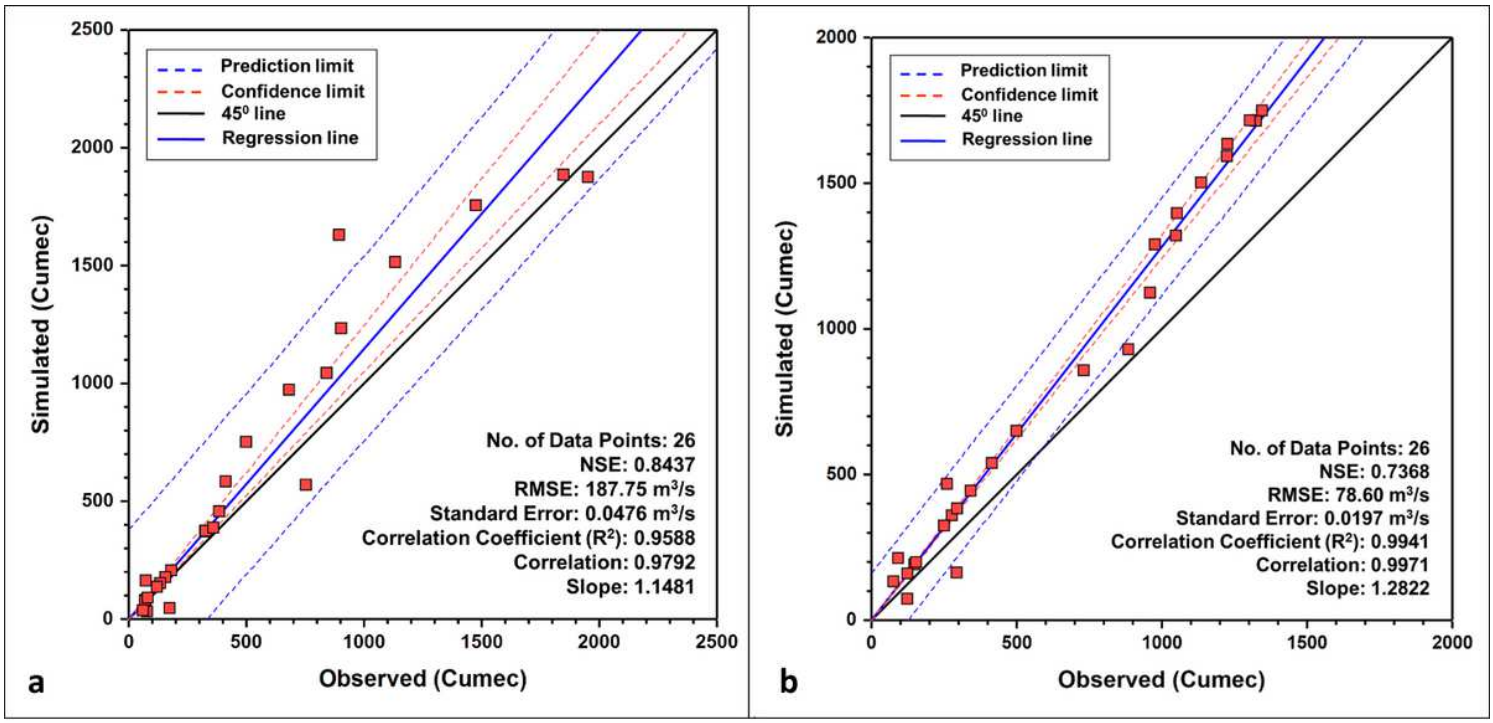

Figure 6

Scattered plots (2014) at other stations: a) RamMunshi Bagh and b) Asham

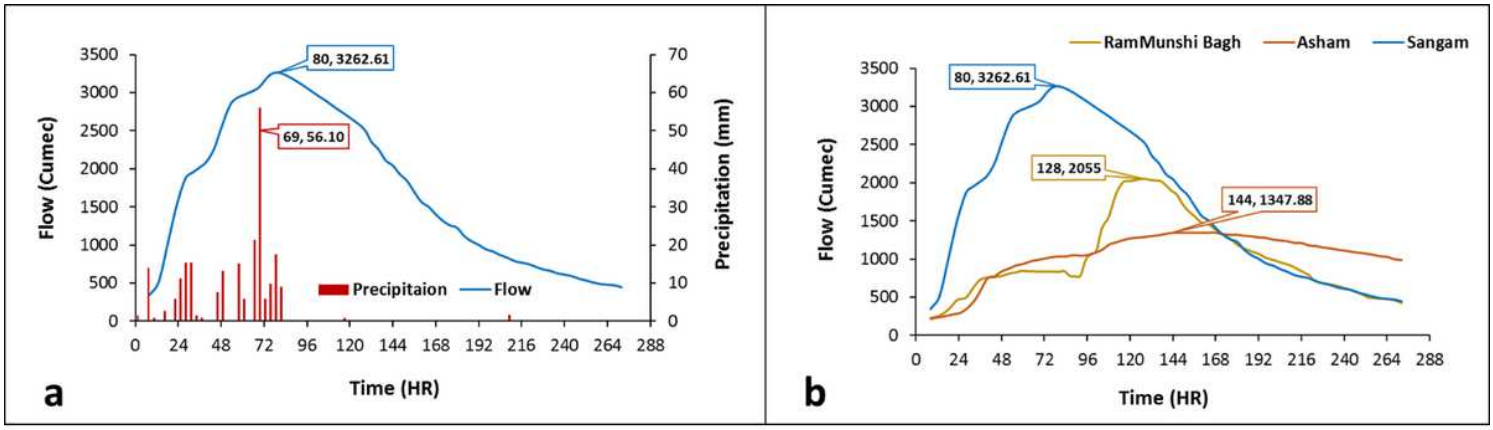

Figure 7

a) Time lag (2014) at Sangam; b) flow (2014) at Sangam, RamMunshi Bagh & Asham

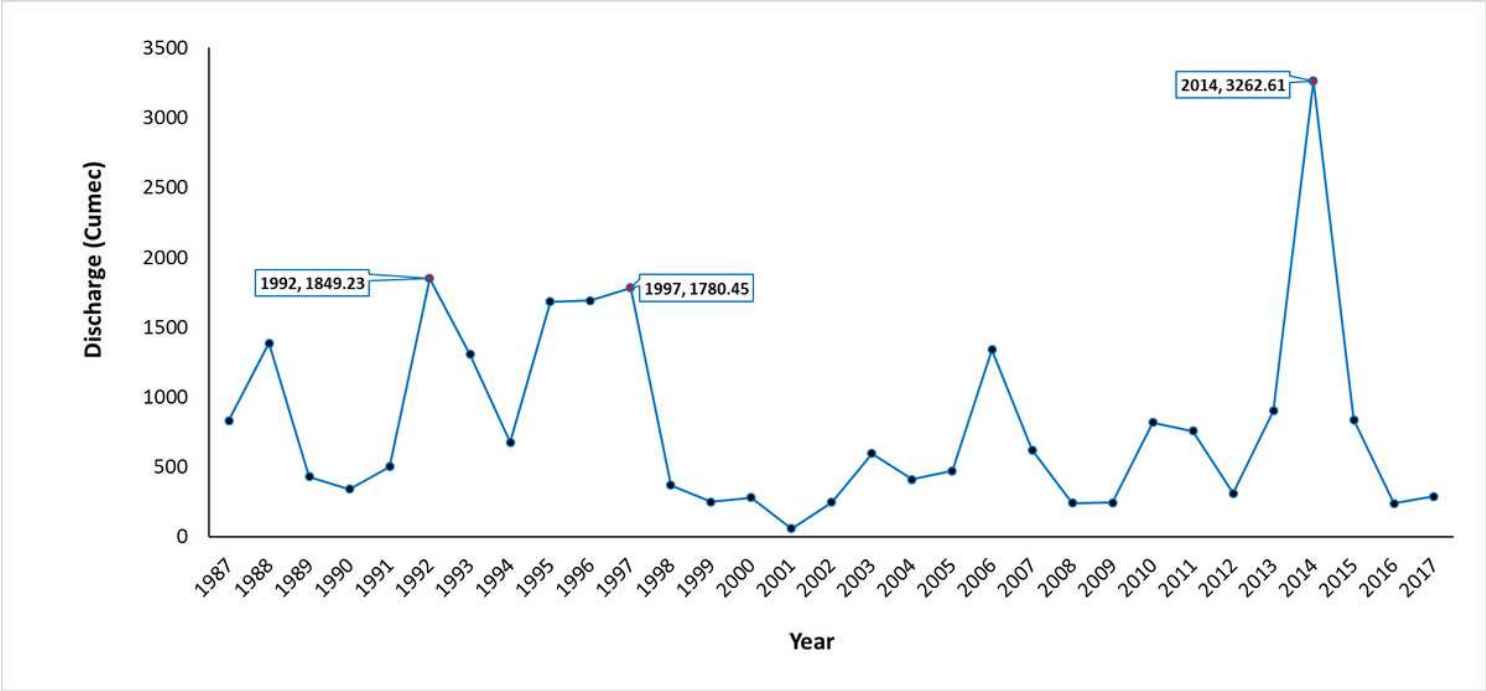

Figure 8

Year wise maximum flow at Sangam

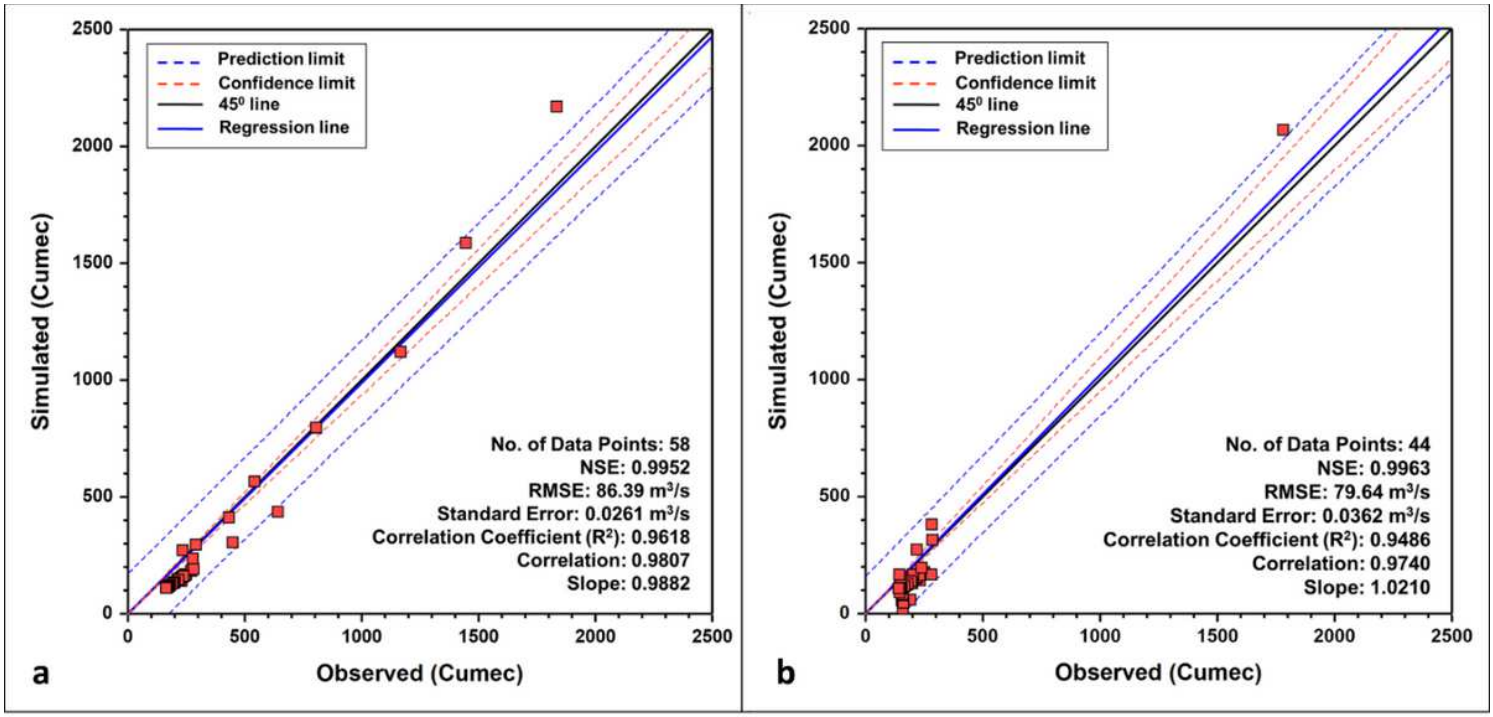

Figure 9

Validation scattered plots at Sangam: a) year 1992 and b) year 1997

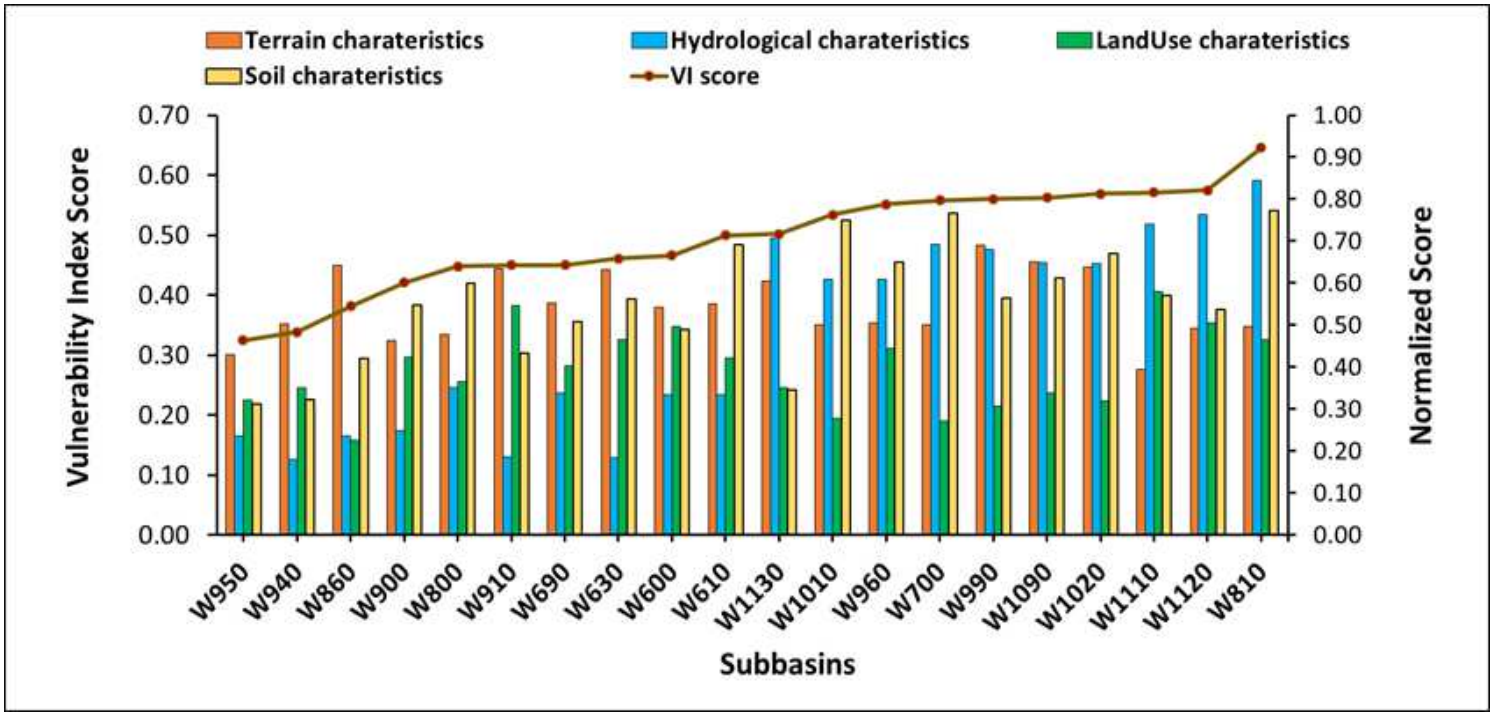

Figure 10

Sub-basins wise Vulnerability Index score plot with their classification using the color ramp representation and the normalized score plot of their characteristics

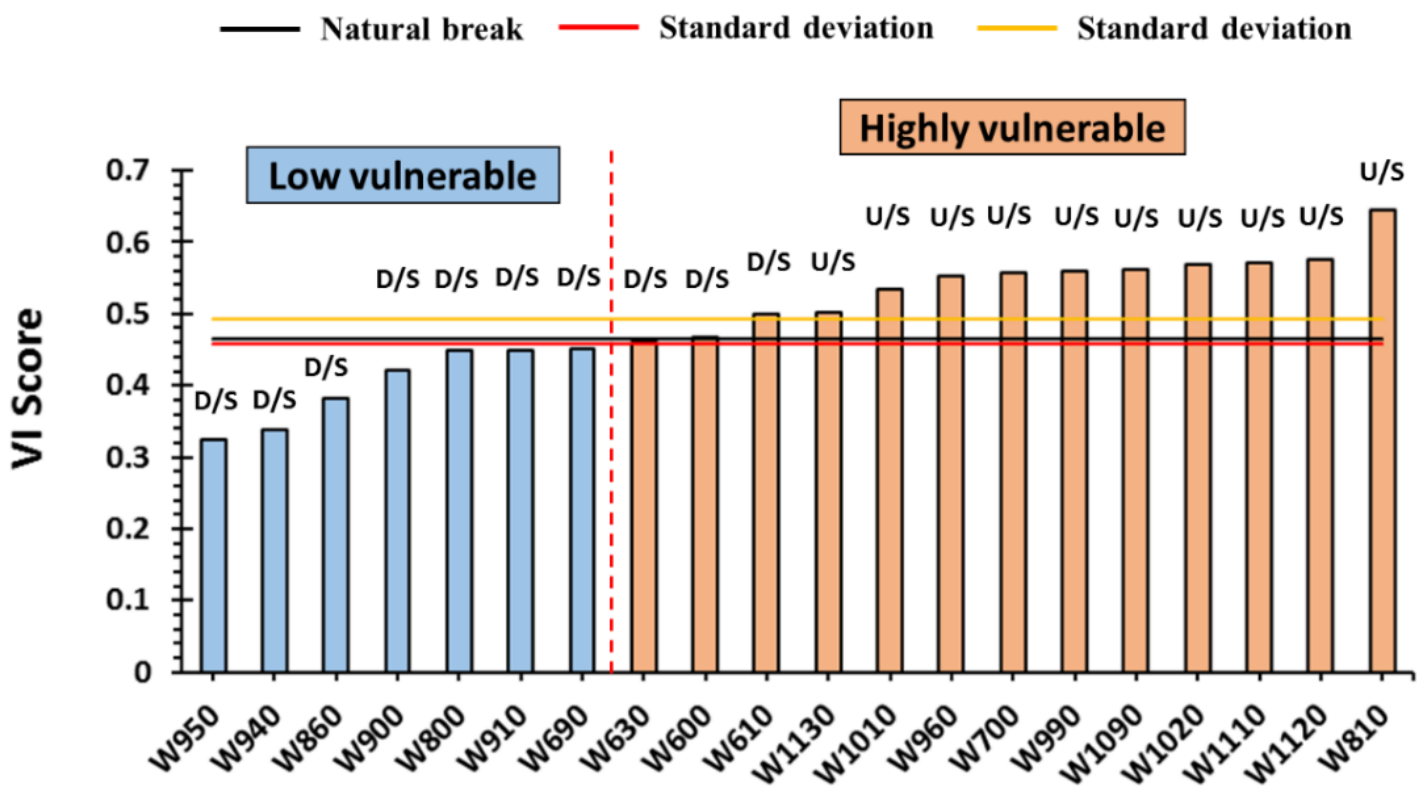

Figure 11

D/S = Downstream (contributing to RamMunshi Bagh and Asham) and U/S = Upstream (contributing to Sangam)

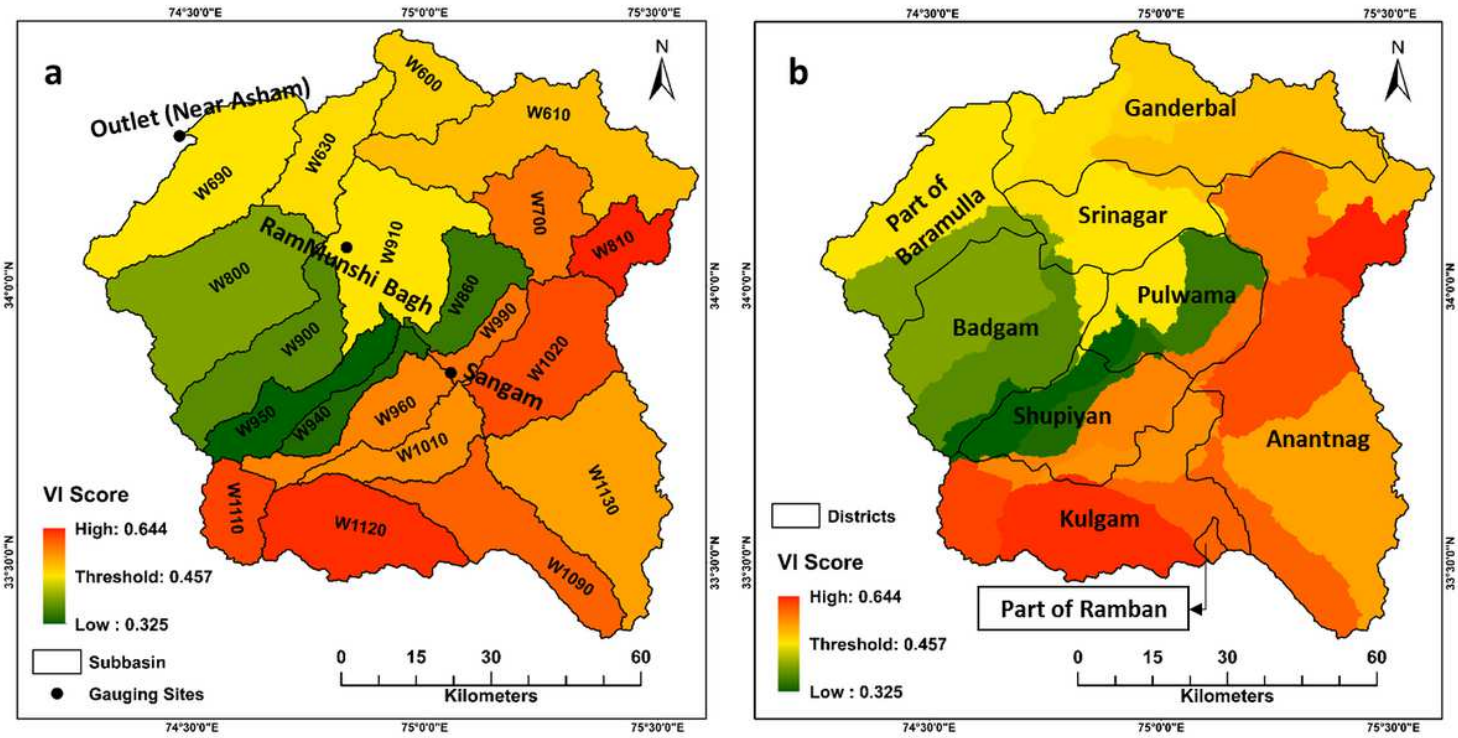

Figure 12

Vulnerability Index score map: a) sub-basins wise, and b) district wise

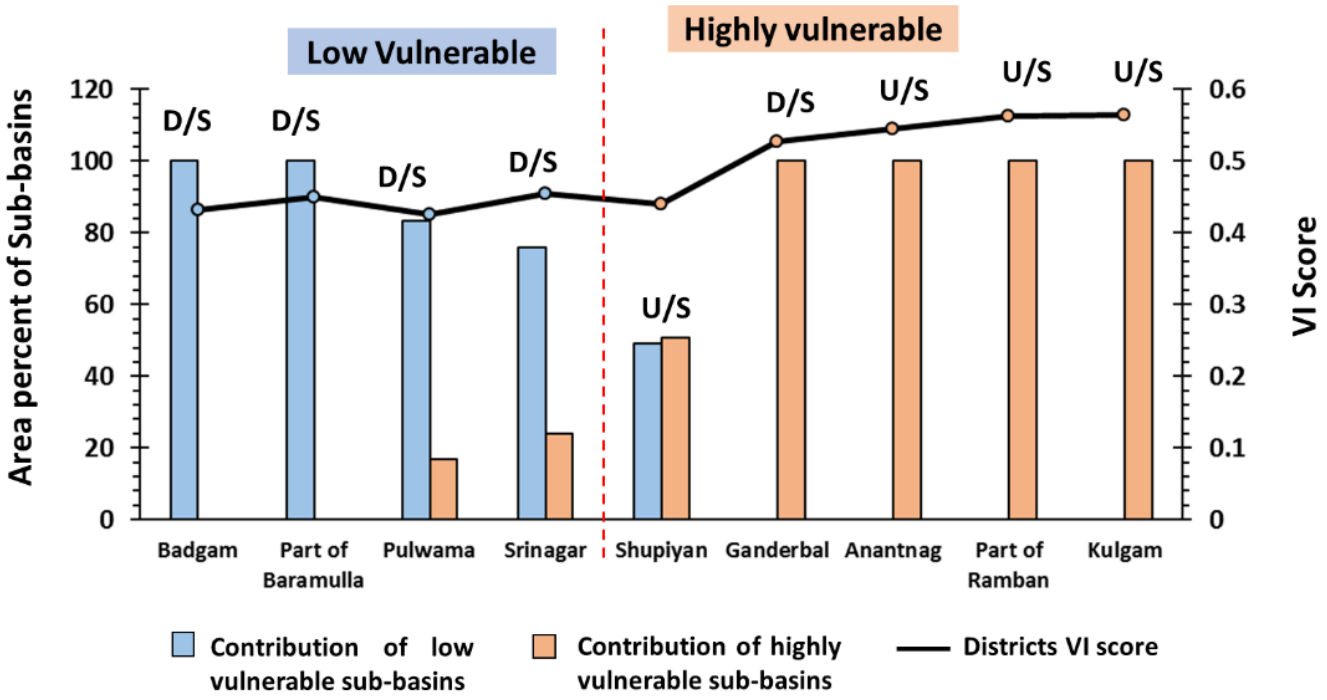

Figure 13

Area contribution of sub-basins in the respective districts and district wise VI score